Available online at www.sciencedirect.com
SCIENCE DIRECT®
Computers and Geotechnics 31 (2004) 491–516
COMPUTERS AND GEOTECHNICS
www.elsevier.com/locate/compgeo

# Bearing capacity of a cohesive-frictional soil under non-eccentric inclined loading

Mohammed Hjiaj *, Andrei V. Lyamin, Scott W. Sloan

*Department of Civil, Surveying and Environmental Engineering, The University of Newcastle, University Drive, Callaghan, NSW 2308, Australia*

Received 19 June 2003; received in revised form 17 June 2004; accepted 18 June 2004

**Abstract**

This paper applies numerical limit analysis to evaluate the bearing capacity of a strip footing, subjected to a non-eccentric inclined load, resting on a ponderable cohesive-frictional soil. Accurate lower and upper bounds are calculated rigorously using finite elements and nonlinear programming. By adopting typical values for the friction angle, the inclination angle, and a dimensionless parameter related to the self-weight, most cases of practical interest are treated. The results are presented in the form of tables. As the gap between the bounds does not exceed 3%, the average limit load provides a good estimate of the exact ultimate load and can be used with confidence for design purposes. The numerical results are compared with ultimate loads predicted by the theories of Meyerhof, Hansen and Vesić. The comparison shows that the Meyerhof and Vesić theories results are unconservative for inclined loading. In particular, the inclination factors from the Meyerhof theory appear to be inaccurate, whilst the Vesić theory does not take proper account of the self-weight. For a ponderable soil under vertical or inclined loading, the collapse mechanism from the rigorous upper bound analysis is different to that assumed by previous authors.


*Keywords:* Bearing capacity; Strip footing; Inclined load; Limit analysis; Finite element; Mathematical programming

## 1. Introduction

The stability of foundations under inclined loads is a fundamental problem in geotechnical engineering. The type of loading, which is often known as combined loading, is particularly important in oil industry where offshore foundations are subjected to vertical and horizontal loads as well as moments. Typically, the vertical force stems from the weight of the superstructure (or a part of it), while the horizontal load comes from wind and wave forces. Generally speaking, the idealized case of a foundation under a central vertical load is a gross simplification of what actually occurs in practice. Even in a simple multistory building, suspended slab floors generate horizontal forces that are transmitted to the foundation by load bearing walls. Fortunately, in these cases, the horizontal forces are usually not comparable in magnitude to the vertical ones and it is often safe to ignore them.

The ultimate bearing capacity of surface strip footing, subjected to an inclined load and resting on a ponderable cohesive-frictional soil, has been studied by numerous investigators. Traditionally, the inclination of the load is taken into consideration through a semi-empirical modification of the theory available for a vertical load. In turn, most of the bearing capacity theories for a vertical load are derived using the superposition principle introduced by Terzaghi [27], which assumes that contributions from the cohesion, the surcharge and the unit weight can be summed independently. Key papers that have influenced various national design standards include those of Meyerhof [14,15], Hansen [11] and Vesić

* Corresponding author. Tel.: +61 2 4921 5582; fax: +61 2 4921 5582.
*E-mail address:* mohammed.hjiaj@newcastle.edu.au (M. Hjiaj).

0266-352X/$ - see front matter © 2004 Elsevier Ltd. All rights reserved.
doi:10.1016/j.compgeo.2004.06.001

[28]. Meyerhof's theory is based on the limit-equilibrium method and is popular in the engineering community because of its simplicity. Hansen's solutions were obtained from the slip-line method, and provided a new expression for the bearing capacity factor $N_\gamma$, with the remaining factors being unchanged. Vesić suggested, a few years later, a slight modification to Hansen's $N_\gamma$ factor. To take into account, the effect of inclined loading, each of the terms in the conventional bearing capacity expression is corrected by a coefficient known as an *inclination factor*. These factors are equal to one for a vertical load and decrease as the inclination angle with respect to the vertical increases. The Meyerhof procedure is simple to apply and makes use explicitly of the inclination angle. The Hansen and Vesić methods both take into account the roughness of the footing, with the latter using modified Hansen expressions for the inclination factors.

Like classical plasticity methods, limit-equilibrium and slip-line procedures both seek to isolate the ultimate load. In the limit-equilibrium method, only global equilibrium is enforced and the shape of the failure mechanism is assumed a priori. Moreover, the kinematics of the problem are ignored in the sense that no strain rate field is defined and the flow rule is not invoked. These characteristics make the limit equilibrium method contentious, even though it is widely used in practice. The slip-line method is based on integrating the equations of plastic equilibrium [25] and is more rigorous, but still takes no account of the flow rule and can only deal with a restricted set of boundary conditions. For problems involving self-weight, this technique gives rise to a hyperbolic set of partial differential equations which must be integrated numerically to obtain the ultimate load [2]. To derive a rigorous lower bound from a slip-line solution, it is necessary to extend the stress field throughout the domain in such a way that it satisfies the equilibrium, yield and stress boundary conditions. This process, which "completes" the stress field, is often laborious and difficult. Complete stress fields give ultimate loads that are usually lower than their incomplete counterparts, as the extension process merely restricts the range of feasible solutions. Besides the approaches recalled above, we may also compute upper bound estimates of the bearing capacity using rigid block mechanisms [26]. In this method, a mechanism composed of rigid blocks is considered and dissipation is assumed to occur only at interfaces between adjacent blocks. Under the assumption of an associated flow rule, it can be proved that the dissipation is a function only of the velocities. This property is used to compute the dissipation along the discontinuities, with the geometry being optimized to yield the minimum dissipated power and the optimum (lowest) collapse load. Drescher and Detournay [8] investigated rigid block mechanisms for frictional materials and suggested that, by adopting reduced strength properties, they could be used to estimate the limit loads for non-associated flow. Because the rigid block method neglects the plastic dissipation within the blocks, it may lead to upper bounds which are too optimistic (especially if the true failure mechanism is complex).

An alternative approach for predicting the stability of geotechnical structures is to use the bound theorems of limit analysis [9]. These assume the soil to be rigid-perfectly plastic with an associated flow rule, and are based on the static and kinematic theorems. The former provides a lower bound for the load multiplier while the latter gives an upper bound. A major advantage of the limit theorems is that the exact collapse load can be bracketed between two values, thus providing an inbuilt estimate of the error in the solutions. Furthermore, the theory is rigorous, since it is based on the equations of continuum mechanics.

Although some exact limit analysis solutions are available for vertical loading of shallow foundations (e.g., strip and circular footings on undrained clay and weightless Coulomb soil), their extension to the general case of vertical and horizontal loading has proved to be difficult. Salençon and Pecker [20,21], who considered a purely cohesive soil with and without tensile strength, used limit analysis to derive (almost) exact solutions for the bearing capacity under non-vertical loading. The utility of the limit theorems can be greatly increased by implementing them in discrete form, for example by employing finite elements. This process, which is adopted here, reduces the task of finding the limit load to one of solving a classical mathematical programming problem and is extremely powerful. To study the bearing capacity of a rigid surface footing resting on a ponderable cohesive-frictional soil under non-eccentric inclined loading, we vary the friction angle, the inclination angle, and a dimensionless material parameter. These quantities are carefully chosen to cover most cases of practical interest. Since the computed upper and lower bounds are sharp, their average gives a good estimate of the exact limit load which can be used with confidence in design. The results suggest that the predictions from the Meyerhof and Vesić theories can be unconservative for non-eccentric inclined loading. This is because the assumption of a one-sided mechanism, which is used to derive their inclination factors, is not always correct.

The rest of the paper is organized as follows. Section 2 defines the problem under consideration, describes the governing equations, and introduces the notation used. In Section 3, the limit analysis theorems are recalled, while Section 4 discusses the mathematical programming problems obtained after discretization by finite elements. Section 5 presents the analytical expressions developed by Meyerhof, Hansen and Vesić, which have influenced standards for designing foundations subjected to inclined load. Numerical results are given in Section 6 and compared with these theories. The paper ends with conclusions.

## 2. Problem definition

The present study investigates the ultimate bearing capacity of a rigid strip footing of width $B$, subjected to an inclined load $\mathbf{Q}$, which is resting on a deep layer of homogeneous cohesive-frictional soil (Fig. 1). It is assumed that the soil is of unit weight $\gamma$, the footing is perfectly rough, and that the non-eccentric force acting upon the foundation is inclined at an angle $\alpha$ with respect to the vertical. Further, the cohesive-frictional soil is assumed to be rigid perfectly plastic and modelled by a Mohr–Coulomb yield criterion with cohesion $c$ and friction angle $\phi$. The length of the footing, denoted by $L$, is supposed to be sufficiently large so that a condition of plane strain exists in the soil mass supporting the foundation. In practice, this assumption is valid provided $B/L \leqslant 1/5$. Under an inclined load, failure can occur either by sliding of the footing along its base or general shear of the underlying soil. If the foundation is perfectly rough, sliding will occur within the soil just beneath the footing and not at the interface. In the following, vectors and matrices are denoted by bold face type, the superimposed dot denotes a derivative with respect to time, and the scalar product is represented by a "·". For plane strain conditions, the static and kinematic variables are:

$$\boldsymbol{\sigma} = \begin{Bmatrix} \sigma_x \\ \sigma_y \\ \tau_{xy} \end{Bmatrix}, \quad \dot{\boldsymbol{\varepsilon}}^p = \begin{Bmatrix} \dot{\varepsilon}_x^p \\ \dot{\varepsilon}_y^p \\ \dot{\varepsilon}_{xy}^p \end{Bmatrix}, \quad \mathbf{v} = \begin{Bmatrix} v_x \\ v_y \end{Bmatrix},$$

where $\boldsymbol{\sigma}$ denotes in-plane Cauchy stresses, $\dot{\varepsilon}^p$ are in-plane plastic strain rates, and $\mathbf{v}$ are the velocities.

In the limit load problem, we find the limit load multiplier $\mu$, the stress field, and the velocity field such that the equations of continuum mechanics are satisfied. Since we are concerned with incipient collapse, all equations are referred to the original undeformed state. Under this assumption, the local equilibrium equations within the domain are

$$\begin{aligned} \frac{\partial \sigma_x}{\partial x} + \frac{\partial \tau_{xy}}{\partial y} &= 0, \\ \frac{\partial \tau_{xy}}{\partial x} + \frac{\partial \sigma_y}{\partial y} &= \gamma. \end{aligned} \tag{1}$$

For a rigid foundation, the surface tractions immediately beneath the footing must satisfy the boundary equilibrium conditions:

$$\begin{aligned} \mu\, V &= -\int_{-B/2}^{B/2} \sigma_y \,\mathrm{d}x = \mu\, \mathbf{Q} \cos\alpha, \\ \mu\, H &= -\int_{-B/2}^{B/2} \tau_{xy} \,\mathrm{d}x = \mu\, \mathbf{Q} \sin\alpha. \end{aligned} \tag{2}$$

Elsewhere on the free surface, we have

$$\mathbf{n}\,\boldsymbol{\sigma} = \mathbf{0}, \tag{3}$$

where $\mathbf{n}$ denotes a $2 \times 3$ matrix comprising components of the outward normal to the free surface. The kinematic relations between velocity and strain rate in a small displacement setting are:

$$\dot{\varepsilon}_x^p = \frac{\partial v_x}{\partial x}, \quad \dot{\varepsilon}_y^p = \frac{\partial v_y}{\partial y}, \quad \dot{\varepsilon}_{xy}^p = \frac{1}{2}\left(\frac{\partial v_x}{\partial y} + \frac{\partial v_y}{\partial x}\right). \tag{4}$$

Rigid body motion of the footing constrains the surface velocities at points along the contact interface. In addition, at some finite distance from the footing, the soil remains rigid and the velocity is equal to zero. To complete the problem statement, the behaviour of the

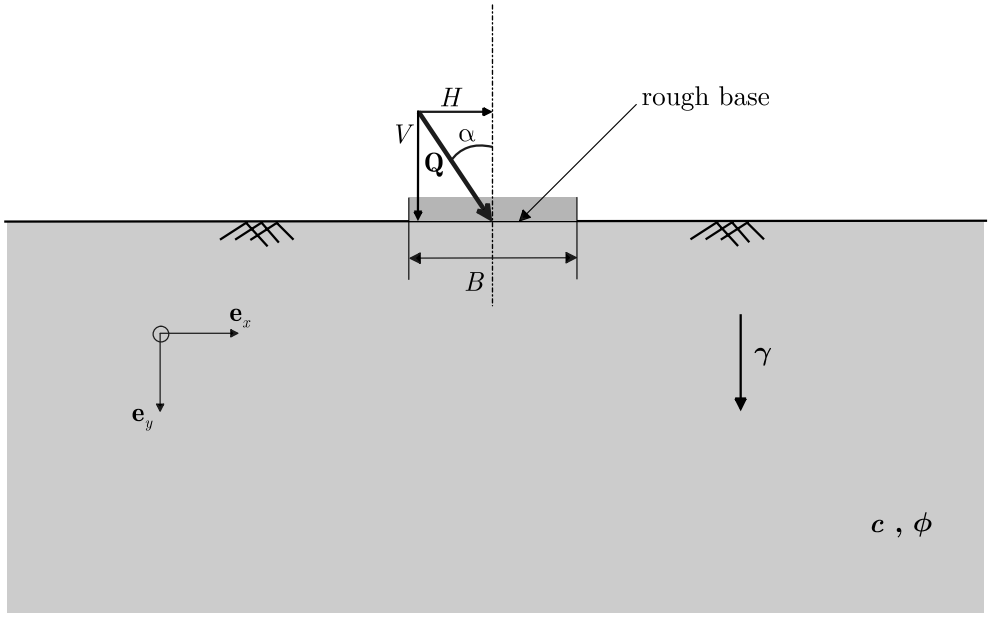


Fig. 1. Strip footing subjected to non-eccentric inclined load.

soil must be specified. The associated Mohr–Coulomb model is adopted. The Mohr–Coulomb yield criterion under plane strain conditions is given by

$$f(\boldsymbol{\sigma}) = \left(\sigma_x - \sigma_y\right)^2 + 4\tau_{xy}^2 - \left(2c\cos\phi + \left(\sigma_x + \sigma_y\right)\sin\phi\right)^2 = 0, \tag{5}$$

where tensile normal stresses are taken as positive. For an associated flow rule, the direction of the plastic strain rate vector is given by the gradient to the yield function, with its magnitude given by the plastic multiplier rate $\dot{\lambda}$:

$$\dot{\varepsilon}^p = \dot{\lambda}\frac{\partial f}{\partial \boldsymbol{\sigma}}. \tag{6}$$

Under plane strain conditions, this becomes:

$$\dot{\varepsilon}_x^p = \dot{\lambda}\frac{\partial f}{\partial \sigma_x}, \quad \dot{\varepsilon}_y^p = \dot{\lambda}\frac{\partial f}{\partial \sigma_y}, \quad \dot{\varepsilon}_{xy}^p = \dot{\lambda}\frac{\partial f}{\partial \tau_{xy}}.$$

To ensure that the yield surface gradient exists everywhere, a smoothed version of the original Mohr–Coulomb criterion is used [1]. In the context of limit analysis, a stress is said to be statically admissible ($\boldsymbol{\sigma}^{sa}$) if it satisfies the equations of internal equilibrium (1), the boundary conditions for the surface tractions (2) and (3) and the yield condition, i.e., $f(\boldsymbol{\sigma}) \leqslant 0$. Similarly, a velocity field is said to be kinematically admissible ($\mathbf{v}^{ka}$) if it satisfies the kinematic relations (4) throughout the domain, the kinematic boundary conditions, the flow rule (6), and leads to a positive value for the power expended by the external loads. A major feature of limit analysis is the inclusion of discontinuities in both the velocity and stress fields. As shown in Fig. 2, a velocity discontinuity corresponds to an intense distortion in the deformation field. The total internal dissipation rate in a kinematically admissible velocity field is computed by summing the dissipation rates that occur in the solid and the velocity discontinuities:

$$P_i(\mathbf{v}) = \int_\Omega \boldsymbol{\sigma}\cdot\dot{\varepsilon}^p(\mathbf{v})\,\mathrm{d}\Omega + \int_{\mathscr{D}} (\mathbf{n}\,\boldsymbol{\sigma})\cdot[\![\mathbf{v}]\!]\,\mathrm{d}\Gamma, \tag{7}$$

where $\Omega$ represents the volume of the half space, $\mathscr{D}$ is any line of discontinuity in the velocity field, and $[\![\mathbf{v}]\!]$ is the discontinuity velocity jump:

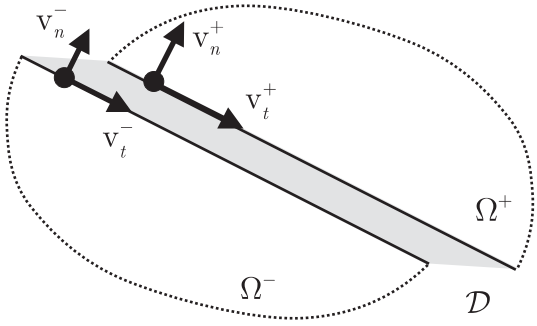


$$\mathbf{v}_n^+ - \mathbf{v}_n^- = \left|\mathbf{v}_t^+ - \mathbf{v}_t^-\right|\tan\phi$$

Fig. 2. Velocity discontinuity.

$$[\![\mathbf{v}]\!] = \mathbf{v}^+ - \mathbf{v}^-.$$

In this equation, $\mathbf{v}^+$ and $\mathbf{v}^-$ denote the velocity on either side of the discontinuity (Fig. 2) and $\mathbf{n}$ is the outward normal to $\mathscr{D}$.

The loading on the footing can be represented either by the resultant force $\mathbf{Q}$ and the inclination angle $\alpha$, or by two statically equivalent forces $V$ and $H$ (Fig. 1):

$$\mathbf{Q} = H\ \mathbf{e}_x + V\ \mathbf{e}_y.$$

Since the footing is rigid, its kinematics are completely specified by the velocity of its center, $\mathbf{v}^0$:

$$\mathbf{v}^0 = v_x^0\ \mathbf{e}_x + v_y^0\ \mathbf{e}_y,$$

where $v_x^0$ and $v_y^0$ are the horizontal velocity and the vertical velocity, respectively. The rate of work expended by the external forces in a kinematically admissible velocity field is then given by:

$$\begin{aligned} P_e(\mathbf{v}) &= \mathbf{Q}\cdot\mathbf{v}^0 + \int_\Omega \gamma v_y\,\mathrm{d}\Omega \\ &= H\ v_x^0 + V\ v_y^0 + \gamma\int_\Omega v_y\,\mathrm{d}\Omega. \end{aligned} \tag{8}$$

By introducing the following notation:

$$\langle v_y\rangle = \int_\Omega v_y\,\mathrm{d}\Omega,$$

(8) can be rewritten as

$$P_e(\mathbf{v}) = H\ v_x^0 + V\ v_y^0 + \gamma\langle v_y\rangle.$$

## 3. Limit analysis theorems

The chief objective of limit analysis is to determine the limit load or load multiplier for a given structure. The technique is based on two theorems, first proposed by Drucker et al. [9], which are recalled below with reference to the present problem. Both theorems assume the flow rule is associated, so that the plastic strain rates are normal to the yield surface. Whilst this assumption predicts excessive dilation upon shear failure, and is often perceived to be a shortcoming for frictional soils, it has little influence on the collapse load for cases that are not strongly constrained in a kinematic sense (e.g. those with a freely deforming surface and a semi-infinite domain). Indeed, for these types of problems, the use of an associated flow rule will usually give good estimates of the ultimate load. This important result is discussed at length by Davis [6] and has been confirmed in a number of independent finite element studies (e.g. [29,23]).

Let the force $\mathbf{Q}$ acting on the footing be of unitary magnitude, so that the problem is now to find the maximum force $\mu\mathbf{Q}$, $\mu$ being a strictly positive parameter, that can be supported by the underlying soil. The upper bound theorem states that the load multiplier deter-

mined by equating the internal rate of dissipation to the external rate of work, for a kinematically admissible velocity field $\mathbf{v}^{ka}$, is not less than the actual collapse load. As a consequence of this theorem, the actual load multiplier is the lowest load multiplier:

$$\mu = \inf_{\mathbf{v}^{ka}} \mu^k(\mathbf{v}), \tag{9}$$

where

$$\mu^k(\mathbf{v}) = \frac{\int_\Omega \boldsymbol{\sigma} \cdot \dot{\varepsilon}^p(\mathbf{v})\,\mathrm{d}\Omega + \int_\Sigma (\mathbf{n}\ \boldsymbol{\sigma}) \cdot [\![\mathbf{v}]\!]\,\mathrm{d}\Sigma - \gamma\langle v_y \rangle}{\mathbf{Q} \cdot \mathbf{v}^0}. \tag{10}$$

The lower bound theorem states that the loads, determined from a stress field that satisfies equilibrium within the domain and on its boundary and does not violate the yield condition, are no greater than the actual collapse load. Accordingly, the limit load is obtained as the supremum:

$$\mu = \sup_{\boldsymbol{\sigma}^{sa}} \mu^s(\boldsymbol{\sigma}). \tag{11}$$

The actual limit load is bracketed by the two load multipliers:

$$\mu^s \leqslant \mu \leqslant \mu^k. \tag{12}$$

The limit theorems are most powerful when both types of solution can be computed so that the actual collapse load can be bracketed closely from above and below. This type of calculation provides a built-in error check on the accuracy of the estimated collapse load and is invaluable when an approximate solution is hard to obtain by other methods. Practical use of these theorems usually requires a numerical method, since analytical bound solutions are available only for a few problems involving simple geometries and basic loading conditions. However, great care has to be taken to preserve the bounding properties of the numerical solution. The most powerful numerical formulations are undoubtedly based on the finite element method, since it allows us to consider problems with complex geometries, non-homogeneous material properties, anisotropy, and various loading conditions. The finite element bound codes UPPER and LOWER, developed in the Newcastle Geotechnical Research Group by Andrei Lyamin and Scott Sloan, are used here.

## 4. Numerical limit analysis

As soon as the limit theorems were established, connections with optimization theory were recognized and limit analysis problems for discrete structures (such as frames) were cast in a linear programming form. In the early 1970s, the applicability of the bound theorems was greatly enhanced by combining them with finite elements and mathematical programming techniques. The resulting methods, which we term finite element bound techniques, inherit all the benefits of the finite element approach and are thus very general.

### 4.1. Discrete formulation of the lower bound theorem

In the lower bound formulation, the stress field is discretized using finite elements with stress nodal variables according to:

$$\boldsymbol{\sigma}(\mathbf{x}) = N_i(\mathbf{x})\boldsymbol{\sigma}_i, \tag{13}$$

where $\boldsymbol{\sigma}_i$ is a nodal stress vector and $N_i$ (**x**) are shape functions. To ensure the yield criterion is satisfied everywhere by enforcing it only at the nodes of each element, the shape functions must be linear (Fig. 3(a)). Linear equality constraints on the nodal stresses arise from the application of the equilibrium equations (1) over each element. By differentiating (13) and substituting into (1), the following linear equality constraints are obtained:

$$\mathbf{A}^e\boldsymbol{\Sigma} = \mathbf{b}^e, \tag{14}$$

where $\boldsymbol{\Sigma}$ is the global vector of nodal stresses, $\mathbf{A}^e$ is a matrix of equality constraint coefficients and $\mathbf{b}^e$ is a vector

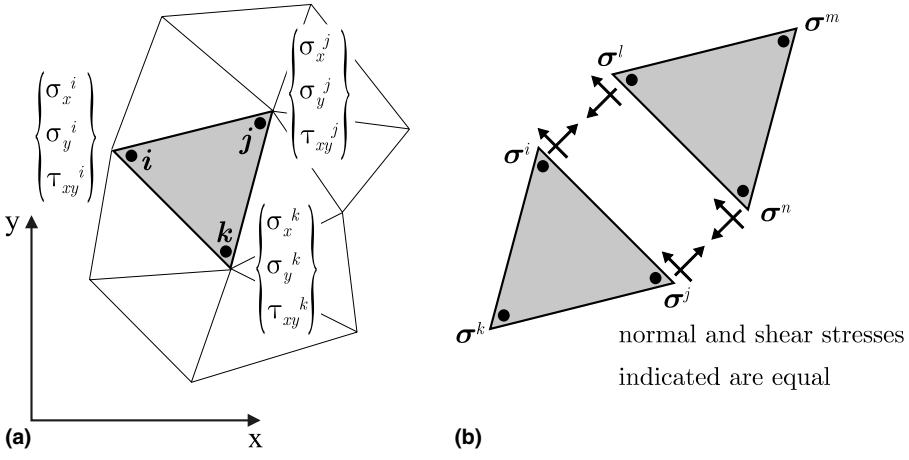


Fig. 3. (a) Linear stress element for lower bound method – (b) Equilibrium of surface tractions between adjacent elements.

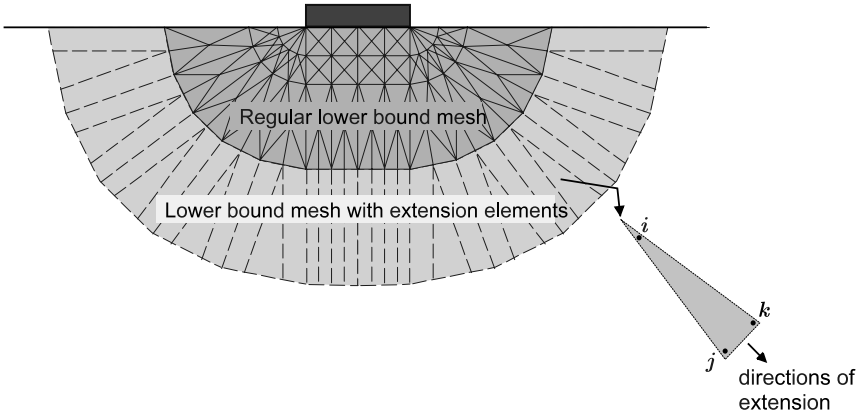


Fig. 4. Extension elements for lower bound method.

of coefficients. Equilibrium of surface tractions on both sides of adjacent triangles must also be enforced. Since the shape functions are linear, this condition is satisfied by matching traction components only at the nodal pairs that have the same coordinates and share the same edge (Fig. 3(b)).

By introducing the standard stress transformation relations, these conditions take the following form:

$$\mathbf{A}^{ed}\boldsymbol{\Sigma} = \mathbf{b}^{ed}. \tag{15}$$

Equilibrium equations on the boundary (2–3) also generate linear equalities

$$\mathbf{A}^{b}\boldsymbol{\Sigma} = \mathbf{b}^{b} \tag{16}$$

that must be added to the previous ones. Summing the equality constraints (14)–(16) we obtain:

$$\mathbf{A}\ \boldsymbol{\Sigma} = \mathbf{b}.$$

Unlike the more familiar displacement finite element method, each node is unique to a particular element (Fig. 3(a)) and, therefore, several nodes may share the same coordinates.

Including statically admissible stress discontinuities along the sides of adjacent elements greatly improves the accuracy of the lower bound solution, as they permit the stress field to change rapidly where needed. To complete the stress field in the deep soil layer (which is a half-space), special extension elements are included in the mesh to satisfy equilibrium, the stress boundary conditions, and the yield criterion throughout the domain (Fig. 4).

The mesh for the lower bound uses a high element density close to the edge of the footing where an abrupt change of boundary conditions occurs (Fig. 5). Indeed, a dense fan of discontinuities, centred on the stress singularity at the edge of the footing, greatly improves the accuracy of the lower bound.

In earlier formulations, nonlinear constraints on the nodal points, arising from the satisfaction of the yield criterion, were avoided by using internal yield surface

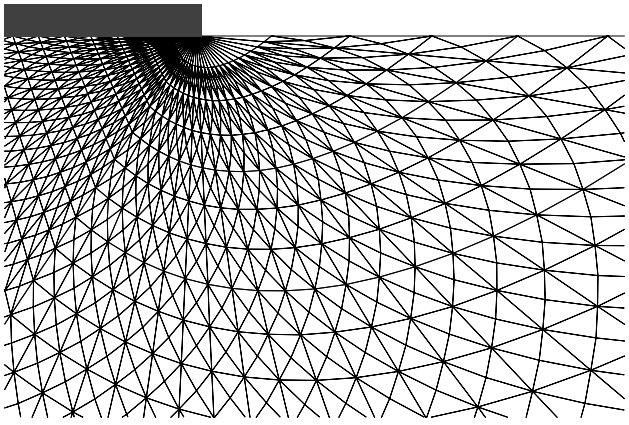

Fig. 5. Mesh refinement near the stress singularity.

linearizations. Although this strategy proved successful for the solution of two-dimensional stability problems, it is unsuitable for three-dimensional geometries. This is because the linearization of a three-dimensional yield surface inevitably generates huge numbers of linear inequalities which, in turn, lead to long solution times for any linear programming solver that conducts a vertex-to-vertex search (such as a simplex or active set method). Another alternative for formulating a lower bound scheme, recently developed by Lyamin and Sloan [13], is to combine linear finite elements with a nonlinear programming solution procedure. This approach uses the yield criterion in its native nonlinear form. Because linearization of the yield surface is avoided, a wide range of convex yield criteria can be used without difficulty. Full details of the formulation, along with references about early formulations, can be found in [13]. The objective function of this nonlinear programming problem, which corresponds to the collapse load, is maximized according to:

$$\begin{aligned} &\text{Maximize} && \mathbf{C}^{\mathrm{T}}\boldsymbol{\Sigma} \\ &\text{Subject to} && \mathbf{A}\ \boldsymbol{\Sigma} = \mathbf{b} \\ & && f_i(\boldsymbol{\sigma}) \leqslant 0 \quad i = \{1, \ldots, n\} \end{aligned} \tag{17}$$

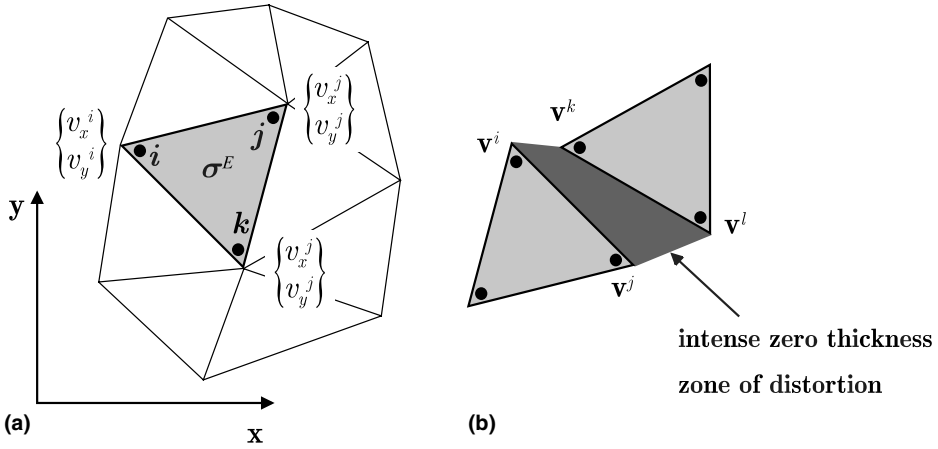


Fig. 6. (a) Upper bound finite element – (b) Kinematically admissible velocity discontinuity.

where $\mathbf{C}$ is a vector of objective function coefficients, $\mathbf{\Sigma}$ is a vector of unknowns (nodal stresses and possibly element unit weights), $\mathbf{C}^{\mathrm{T}}\mathbf{\Sigma}$ is the collapse load, $f_i(\boldsymbol{\sigma})$ is the yield function for node $i$, and $n$ is the number of nodes. The solution to the mathematical problem (17), which constitutes a statically admissible stress field, can be found efficiently by solving the system of nonlinear equations that define its Kuhn–Tucker optimality conditions. The two-stage quasi-Newton solver used for this purpose usually requires less than about 50 iterations, regardless of the problem size, and the resulting formulation is many times faster than an equivalent linear programming formulation [13].

### 4.2. Discrete formulation of the upper bound theorem

The minimum principle (9) can be cast in discrete form by expressing the velocity field as a function of a finite number of parameters. Plane finite elements with velocity approximations are employed here for this purpose. In each element $E$ ($E = 1,\ldots,N_E$) the velocities are expressed as $\mathbf{v}(\mathbf{x}) = N_i(\mathbf{x})\ \mathbf{v}_i$, where $\mathbf{v}_i$ is a nodal velocity vector and $N_i(\mathbf{x})$ are shape functions. The linear three-noded triangle is used to model the velocity field, as this permits the flow rule, which is expressed in terms of constant plastic strain rates, to be satisfied everywhere within each element. In the upper bound formulation of Lyamin and Sloan [12], which is employed here, each node has two unknown velocities and each element is associated with a single plastic multiplier rate and a constant stress vector (Fig. 6(a)). Kinematically admissible velocity discontinuities are included along all shared element edges in the mesh (Fig. 6(b)). This improves the upper bound solutions, avoids locking (which may occur for incompressible flow), and chooses the direction of shearing automatically during the minimization process to give the least amount of dissipated power [24]. To avoid the Kuhn–Tucker optimality constraints, Lyamin and Sloan [12] transform the minimum problem into a min–max problem. As a result of this transformation, the plastic multiplier rate does not appear explicitly in the formulation, thus reducing the size of the problem.

Once the constraints and objective function coefficients are assembled, the task of finding a kinematically admissible velocity field, which minimizes the internal power dissipation for a specified set of boundary conditions, may be written as

$$\begin{aligned} \underset{\mathbf{\Sigma}}{\text{Maximize}} \quad \underset{\mathbf{V},\mathbf{D}}{\text{Minimize}} \quad & \mathbf{\Sigma}^{\mathrm{T}}\mathbf{B}\mathbf{V} + \mathbf{C}_u^{\mathrm{T}}\mathbf{V} + \mathbf{C}_d^{\mathrm{T}}\mathbf{D} \\ \text{Subject to} \quad & \mathbf{A}_u\mathbf{V} + \mathbf{A}_d\mathbf{D} = \mathbf{b} \\ & f_i(\boldsymbol{\sigma}) \leqslant 0, \quad E = \{1,\ldots,N_E\}, \\ & \mathbf{D} \geqslant 0 \end{aligned} \tag{18}$$

where $\mathbf{V}$ is a global vector of unknown velocities, $\mathbf{D}$ is a global vector of unknown discontinuity variables, $\mathbf{\Sigma}$ is a global vector of unknown element stresses, $\mathbf{C}_u$ and $\mathbf{C}_d$ are vectors of objective function coefficients for the nodal velocities and discontinuity variables, $\mathbf{A}_u$ and $\mathbf{A}_d$ are matrices of equality constraint coefficients for the nodal velocities and discontinuity variables, $\mathbf{B}$ is a global matrix of compatibility coefficients that operate on the nodal velocities, $\mathbf{b}$ is a vector of coefficients, $f_i(\sigma)$ is the yield function for element $i$ and $N_E$ is the number of triangular elements. The objective function $\mathbf{\Sigma}^{\mathrm{T}}\mathbf{B}\mathbf{V} + \mathbf{C}_u^{\mathrm{T}}\mathbf{V} + \mathbf{C}_d^{\mathrm{T}}\mathbf{D}$ corresponds to the total dissipated power, with the first term giving the dissipation in the continuum, the second term giving the dissipation due to fixed boundary tractions or body forces, and the third term giving the dissipation in the discontinuities. The solution to the optimization problem (18), which defines a kinematically admissible velocity field, can be computed efficiently by solving the system of nonlinear equations that define its Kuhn–Tucker optimality conditions. The two-stage quasi-Newton solver used for this purpose has been described in detail by Lyamin and Sloan [12], and is a variant of the scheme developed for their nonlinear lower bound method. It typically

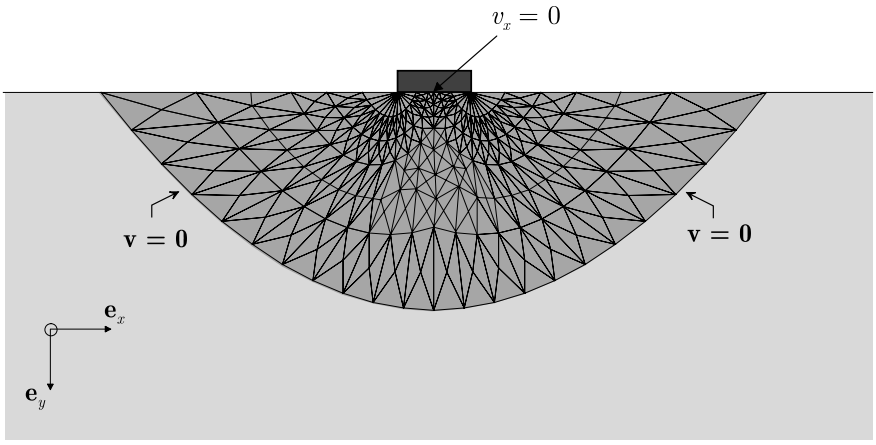


Fig. 7. Typical upper bound mesh.

requires less than about 50 iterations, and results in a formulation which, for large two-dimensional applications, is roughly two orders of magnitude faster than an equivalent linear programming formulation [12].

A typical mesh for the upper bound analysis is based on a geometric arrangement similar to that of the Prandtl–Hill mechanism, with the size of the discretized domain being large enough to contain the potential failure surface (see Fig. 7). Outside the mesh, no plastic deformation takes place and all points are assumed to have zero velocity. If the mesh is made too small, the computed upper bound will still be valid but will greatly overestimate the true collapse load.

The discrete limit analysis formulations described above are used here to estimate the bearing capacity of a surface footing subjected to an inclined load. The true ultimate load is bracketed to within 2.81%. Before presenting results, we now recall the bearing capacity expressions developed by Meyerhof, Hansen and Vesić, which are widely used in practice.

## 5. Bearing capacity theories for inclined loading

The ultimate load for a strip footing subjected to inclined loading can be estimated using bearing capacity factors or published failure envelopes. In the former method, Terzaghi's bearing capacity equation for a strip footing under a central vertical load is modified by empirical factors to account for the inclination of the loading. A number of authors have derived expressions for these factors using limit equilibrium or slip-line procedures. The second approach seeks to characterize a failure envelope, or interaction diagram, that defines all safe load combinations [19]. As a consequence of the associated flow rule assumption, this "failure" surface is convex and the normality rule yields back the foundation velocity at failure. An exact definition of this surface requires an analytical solution of the limit analysis problem, which is not available for the general case of combined loading of a footing on frictional soil. Thus, mostly semi-empirical expressions for the failure envelope have been proposed in the literature, often based on experimental results [10]. The failure envelope approach is not only direct, but also provides an overall picture of the safe load domain.

### 5.1. Bearing capacity factors

During the last 50 years, a variety of theories have been proposed for estimating the ultimate bearing capacity of shallow foundations. Most of these rely on the *superposition* principle suggested by Terzaghi [27], in which bearing capacity contributions from the cohesion, the surcharge, and the unit weight are summed. For a strip footing loaded vertically in the plane of symmetry, the ultimate bearing pressure $q_u$ is represented by the expression

$$q_u = cN_c + qN_q + \tfrac{1}{2}\gamma B N_\gamma, \tag{19}$$

where the bearing capacity factors $N_c$, $N_q$ and $N_\gamma$ represent the effects due to soil cohesion $c$, surface loading $q$, and soil unit weight $\gamma$, respectively. These parameters $N$ are all functions of the internal friction angle $\phi$. Terzaghi's theory is an extension of the analytical work of Prandtl [17] and Reissner [19], who provided the first two terms in (18). Their solution was later shown to be exact, as it satisfies both the upper and lower bound theorems of plasticity theory. To derive his expressions for the bearing capacity factors, Terzaghi applied the limit equilibrium method and adopted Prandtl's failure mechanism. This mechanism comprises three distinct zones: a rigid active wedge beneath the footing, a fan of plastic shearing centred on the edge of the footing, and a rigid passive wedge adjacent to the footing. For a rough footing, the bearing capacity factors may be written as:

$$N_q = \frac{e^{2(3\pi/4-\phi/2)\tan\phi}}{2\cos^2(\pi/4+\phi/2)},$$

$$N_c = (N_q - 1)\cot\phi,$$

$$N_\gamma = \frac{\tan\phi}{2}\left(\frac{K_{p\gamma}}{\cos^2\phi} - 1\right),$$

where $K_{p\gamma}$ is a passive earth pressure coefficient. Whilst the expressions for $N_c$ and $N_q$ are exact for a weightless soil, the precise value for $N_\gamma$ depends on $K_{p\gamma}$. This, in turn, depends on the approximate technique that is used to estimate it.

Although much debate has centred on the correct value for $N_\gamma$, it is clear that the principle of superposition will give only approximate results in any case since the behaviour is nonlinear. The reason for invoking this principle is largely due to convenience, as well as the fact that it avoids many mathematical difficulties when applying the conventional limit equilibrium method. Even though many authors have questioned the accuracy of superposition, no alternative theoretical approach has gained widespread acceptance. Furthermore, the use of superposition often leads to predictions that are on the safe side [7].

In the vast literature on the bearing capacity of shallow foundations, numerous analytical expressions for the factors $N$ have been proposed. Indeed, Vesić [28] tabulated 15 different solutions since 1940. Of these, the solutions due to Meyerhof [14], Hansen [11], and Vesić [28] are the most widely used in practice.

In 1951, Meyerhof [14] published a bearing capacity solution, based on the limit equilibrium method, which is applicable to rough shallow and rough deep foundations. His theory employs a failure surface that takes into account the shearing resistance of the overburden. Neglecting this extra resistance, as advocated by Terzaghi, is normally justified on the grounds that the overburden soil is much weaker than the bearing stratum. Moreover, the solution so obtained will tend to give conservative results. Following Meyerhof's work, Hansen [11] used the slip-line method and provided a new expression for the $N_\gamma$ factor, with the other bearing capacity factors being unchanged. A few years later, Vesić [28] suggested a slightly modified formula which is a closed-form approximation of an earlier slip-line solution by Caquot and Kérisel [4]. Table 1 summarizes the bearing capacity factors derived by each of the above authors.

Table 1
Expressions for bearing capacity factors

| Author | $N_q$ | $N_c$ | $N_\gamma$ |
|---|---|---|---|
| Meyerhof | $e^{\pi\tan\phi}\tan^2(\pi/4+\phi/2)$ | $(N_q-1)\cot\phi$ | $(N_q-1)\cot(1.4\phi)$ |
| Hansen | $e^{\pi\tan\phi}\tan^2(\pi/4+\phi/2)$ | $(N_q-1)\cot\phi$ | $1.5(N_q-1)\tan\phi$ |
| Vesić | $e^{\pi\tan\phi}\tan^2(\pi/4+\phi/2)$ | $(N_q-1)\cot\phi$ | $2(N_q+1)\tan\phi$ |

### 5.2. Inclination factors

Under an inclined load, failure can occur either by sliding of the footing along its base or by general shear of the underlying soil. At the point of sliding, the horizontal component $H$ is related to the vertical component $V$ by $H = Bc + V\tan\phi$.

To estimate the ultimate load for the case of general shear failure, i.e. when $H < Bc + V\tan\phi$, previous authors have modified the original bearing capacity equation (established for a purely vertical load) using semi-empirical coefficients. These modifications typically give an expression of the form

$$q_u = cN_c i_c + qN_q i_q + \frac{1}{2}\gamma \mathrm{B} N_\gamma i_\gamma, \tag{20}$$

where $i_c$, $i_q$ and $i_\gamma$ are inclination factors and $q_u$ is the ultimate vertical bearing pressure, referred to as bearing capacity herein.

In 1953, Meyerhof [15] extended his theory for ultimate bearing capacity under vertical load to the case with inclined load. The assumed failure mechanism is confined to one side of the footing for all values of the inclination angle, and is composed of three zones whose geometry is changed to account for the load inclination. Furthermore, two slightly different mechanisms are considered, one for small inclinations and another for large inclinations. Using the slip-line method, Hansen [11] also derived expressions for the inclination factors. He again assumed a one-sided mechanism and accounted for adhesion $a$ between the soil and the footing base. Soon after, Vesić [28] proposed empirical modifications to Hansen's expressions for the inclination factors and compared their predictions against experimental results. One advantage of the Vesić formulae over the Hansen formulae is that all the parameters appearing in the inclination factors are defined by the material properties and the geometry of the footing, with no empirical factors being needed. Table 2 summarizes the expressions for the inclination factors proposed by each of the above authors.

**Remarks.**

- For a perfectly rough footing, the adhesion $a$ is taken equal to the cohesion $c$.
- Meyerhof's expression for $i_\gamma$ is meaningful only for $\alpha<\phi$.
- Hansen uses 5 for both $\delta_1$ and $\delta_2$, while Bowles [3] recommends $2\leqslant\delta_1\leqslant3$ and $3\leqslant\delta_2\leqslant4$. Hansen's values are adopted in this paper.
- In the formulation of Vesić, $B/L = 0$ for a strip footing.

Table 2
Expressions for inclination factors

| Author | $i_q$ | $i_c$ | $i_\gamma$ | Comments |
|---|---|---|---|---|
| Meyerhof | $\left(1-\frac{\alpha^\circ}{90^\circ}\right)^2$ | $\left(1-\frac{\alpha^\circ}{90^\circ}\right)^2$ | $\left(1-\frac{\alpha^\circ}{\phi^\circ}\right)^2$ | $\alpha<\phi$ |
| Hansen | $\left(1-\frac{0.5H}{V+BLa\cot\phi}\right)^{\delta_1}$ | $\frac{i_qN_q-1}{N_q-1}$ | $\left(1-\frac{0.7H}{V+BLa\cot\phi}\right)^{\delta_2}$ | $2\leqslant\delta_1\leqslant5,2\leqslant\delta_2\leqslant5$ |
| Vesić | $\left(1-\frac{H}{V+BLa\cot\phi}\right)^{m}$ | $\frac{i_qN_q-1}{N_q-1}$ | $\left(1-\frac{H}{V+BLa\cot\phi}\right)^{m+1}$ | $m=\frac{2+B/L}{1+B/L}$ |

A survey of European methods for estimating the bearing capacity of shallow foundations has been carried out by Sieffert and Bay-Gress [22]. This reveals that many European countries make explicit use of the procedures described above.

## 6. Parametric study and discussion

### 6.1. Dimensionless parameters of the problem

The bearing capacity of a surface foundation depends not only on the mechanical properties of the soil (cohesion $c$, friction angle $\phi$ and unit weight $\gamma$), but also on the footing width $B$. Cox [5] showed that, for a smooth surface footing resting on a Mohr–Coulomb soil with no surcharge, the fundamental dimensionless parameters associated with the stress characteristic equations are the friction angle $\phi$ and a weight parameter $G=\gamma B/2c$. If $G$ is small the soil behaves essentially as a cohesive-frictional weightless medium. If $G$ is large soil weight, rather than cohesion, is the principal source of bearing strength. In practice, we can expect that $0^\circ\leqslant\phi\leqslant45^\circ$ and $0\leqslant G\leqslant3$. These limits assume that $\gamma$ varies between 15 and 30 kN/m$^3$, $c$ ranges from 10 to 50 kN/m$^2$, and the footing width ranges from 0.3 to 20 m. In the following, numerical results are presented for $G$ equal to 0, 0.5, 1, 1.5, 2, 2.5 and 3 and $\alpha$ equal to 7.5°, 15°, 22.5°, 30° and 45°. For convenience and completeness, Tables of the predictions are also given.

### 6.2. Results and discussion

Unlike the limit equilibrium method, the discrete formulation of the kinematic theorem does not require the failure mode to be assumed a priori. Rather, it is computed as part of the upper bound solution process. Nevertheless, an appropriate mesh pattern and a careful refinement strategy are essential to achieve numerically accurate solutions. The computed lower and upper bounds on the normalized bearing capacity (average pressure), $V_{UB}:=/cB$ and $V_{UB}:=V_{UB}/cB$, are given in Tables 4–10 for inclination angles up to 45°. Note that for greater load inclinations, sliding occurs for any value of the internal friction angle. In the tables, underlined numbers correspond to failure by sliding. Because the bounds are sharp, very good estimates of the exact ultimate bearing pressure can be obtained by averaging the computed upper and lower bound pressures according to $\tilde{V}_{Av}=(\tilde{V}_{LB}+\tilde{V}_{UB})/2$. Indeed, for the results presented here, the errors defined by

$$\pm50(\tilde{V}_{UB}-\tilde{V}_{LB})/\tilde{V}_{Av} \tag{21}$$

do not exceed ±2.81%. This implies that the maximum difference between the exact solution and the average of the lower/upper bounds is smaller than ±2.81%.

In Meyerhof's theory, the inclination factors depend explicitly on the friction angle and the inclination of the load, so that the ultimate bearing pressure can be calculated directly and compared with the numerical predictions. The procedure is different in the Hansen and Vesić formulas, as their inclination factors involve both the horizontal and the vertical components of the applied load. Accordingly, to compute the ultimate bearing capacity with these methods, the average horizontal and vertical forces found from the numerical limit loads are used. The resulting bearing capacity is then compared with the average numerical bearing capacity.

#### 6.2.1. The vertical loading case

For a vertically loaded footing resting on weightless cohesive-frictional soil, the bearing capacity theory of Prandtl [17] gives the exact result. The numerical bounds, presented in Table 3, are very sharp for this case with a maximum actual percentage error of −1.73% for the lower bound and +2.85% for the upper bound. The same results, but presented differently in Table 4, indi-

Table 3
Comparison between Prandtl's solution and numerical limit analysis

| $\phi$ (°) | Exact | Actual % error LB | Actual % error UB |
|---|---|---|---|
| 5 | 6.49 | −0.26 | +1.04 |
| 10 | 8.34 | −0.41 | +1.41 |
| 15 | 10.98 | −0.73 | +1.54 |
| 20 | 14.83 | −0.88 | +1.99 |
| 25 | 20.72 | −1.21 | +2.27 |
| 30 | 30.14 | −1.32 | +2.45 |
| 35 | 46.12 | −1.35 | +2.51 |
| 40 | 75.31 | −1.28 | +2.54 |
| 45 | 133.87 | −1.73 | +2.85 |

Table 4
Lower and upper bounds on the normalized bearing capacity pressure $VlcB$ for weightless soil

| $\phi$ (°) | $\alpha = 0°$ | | | | $\alpha = 7.5°$ | | | |
|---|---|---|---|---|---|---|---|---|
| | LB | UB | Average | ±Error (%) | LB | UB | Average | ±Error (%) |
| 5 | 6.47 | 6.56 | 6.51 | 0.65 | 5.44 | 5.51 | 5.48 | 0.68 |
| 10 | 8.31 | 8.46 | 8.39 | 0.91 | 6.92 | 6.99 | 6.95 | 0.52 |
| 15 | 10.90 | 11.15 | 11.02 | 1.13 | 8.99 | 9.10 | 9.04 | 0.62 |
| 20 | 14.70 | 15.13 | 14.92 | 1.43 | 11.96 | 12.18 | 12.07 | 0.90 |
| 25 | 20.47 | 21.19 | 20.83 | 1.73 | 16.40 | 16.70 | 16.55 | 0.92 |
| 30 | 29.74 | 30.88 | 30.31 | 1.87 | 23.24 | 23.83 | 23.53 | 1.25 |
| 35 | 45.50 | 47.28 | 46.39 | 1.92 | 34.69 | 35.63 | 35.16 | 1.34 |
| 40 | 74.35 | 77.23 | 75.79 | 1.90 | 55.16 | 57.05 | 56.11 | 1.69 |
| 45 | 131.56 | 137.69 | 134.63 | 2.28 | 93.45 | 98.58 | 96.01 | 2.67 |
| | $\alpha = 15°$ | | | | $\alpha = 22.5°$ | | | |
| 5 | 4.25 | 4.33 | 4.29 | 0.94 | 3.03 | 3.04 | 3.04 | 0.25 |
| 10 | 5.38 | 5.47 | 5.42 | 0.87 | 3.85 | 3.88 | 3.87 | 0.44 |
| 15 | 6.93 | 7.04 | 6.99 | 0.81 | 4.96 | 5.03 | 4.99 | 0.65 |
| 20 | 9.13 | 9.33 | 9.23 | 1.10 | 6.51 | 6.63 | 6.57 | 0.89 |
| 25 | 12.37 | 12.67 | 12.52 | 1.23 | 8.74 | 8.92 | 8.83 | 1.00 |
| 30 | 17.29 | 17.79 | 17.54 | 1.43 | 12.09 | 12.43 | 12.26 | 1.41 |
| 35 | 25.13 | 26.07 | 25.60 | 1.83 | 17.36 | 18.02 | 17.69 | 1.88 |
| 40 | 38.95 | 40.65 | 39.80 | 2.13 | 26.15 | 27.38 | 26.77 | 2.31 |
| 45 | 63.54 | 67.03 | 65.28 | 2.67 | 41.70 | 43.95 | 42.82 | 2.62 |
| | $\alpha = 30°$ | | | | $\alpha = 45°$ | | | |
| 5 | 2.04 | 2.05 | 2.05 | 0.25 | 1.10 | 1.10 | 1.10 | 0.35 |
| 10 | 2.49 | 2.51 | 2.50 | 0.31 | 1.21 | 1.22 | 1.22 | 0.37 |
| 15 | 3.21 | 3.24 | 3.22 | 0.37 | 1.37 | 1.38 | 1.37 | 0.39 |
| 20 | 4.24 | 4.29 | 4.27 | 0.63 | 1.57 | 1.59 | 1.58 | 0.41 |
| 25 | 5.69 | 5.79 | 5.74 | 0.82 | 1.87 | 1.89 | 1.88 | 0.44 |
| 30 | 7.83 | 8.05 | 7.94 | 1.39 | 2.37 | 2.39 | 2.38 | 0.42 |
| 35 | 11.12 | 11.45 | 11.29 | 1.47 | 3.31 | 3.34 | 3.33 | 0.52 |
| 40 | 16.48 | 17.20 | 16.84 | 2.13 | 4.90 | 5.02 | 4.96 | 1.22 |
| 45 | 25.78 | 27.14 | 26.46 | 2.56 | 7.51 | 7.77 | 7.64 | 1.65 |

cate that the bounding error (21) is ±2.28% for the highest friction angle of 45°. We should also mention that accurate results have been obtained by Michałowski using the rigid-block method [16].

The results in Table 3 suggest that the lower bound calculations are more accurate. This is generally the case, as the upper bound predictions are more sensitive to the mesh pattern. To obtain accurate upper bounds for this case, the velocity discontinuities need to follow a log-spiral curve in the lateral direction (see Fig. 8). The decrease in accuracy with increasing friction angle $\phi$ can be attributed to the density of the mesh. Since the number of elements used is approximately constant for all calculations, the mesh density becomes coarser as the size of the plastic zone increases (with increasing friction angle) and is therefore less able to capture changes in the stress and the velocity fields. As expected, the unit weight increases the ultimate bearing capacity of a footing dramatically. To illustrate the effect of self-weight, Fig. 9 shows a plot of the ultimate bearing capacity for a ponderable soil, divided by that of its imponderable counterpart, for various values of the parameter $G$. This figure reveals that the ultimate bearing capacity for a soil with $G = 0.5$ and $\phi = 45°$ is more than double that of a weightless soil with the same friction angle. For a weightier soil ($G = 3$) with the same friction angle, the corresponding increase is a factor of about 7. Fig. 9 suggests that, for a fixed friction angle, the gain in bearing capacity increases linearly with respect to $G$, allowing us to calculate the bearing capacity for intermediate values of $G$ by simple linear interpolation. As expected, the rate of increase in bearing capacity increases with increasing friction angle.

To compare the results from the Meyerhof, Hansen and Vesić theories with those from numerical limit analysis, we define the relative error in the theoretical limit loads $\tilde{V}_{Th}$ as:

$$\frac{\tilde{V}_{Av} - \tilde{V}_{Th}}{\tilde{V}_{Av}}. \tag{22}$$

This measure gives a positive relative error if a theory is conservative and a negative one if the theory is unconservative. However, because it is based on the averaged numerical limit loads, it is meaningful only for errors which exceed about ±3%.

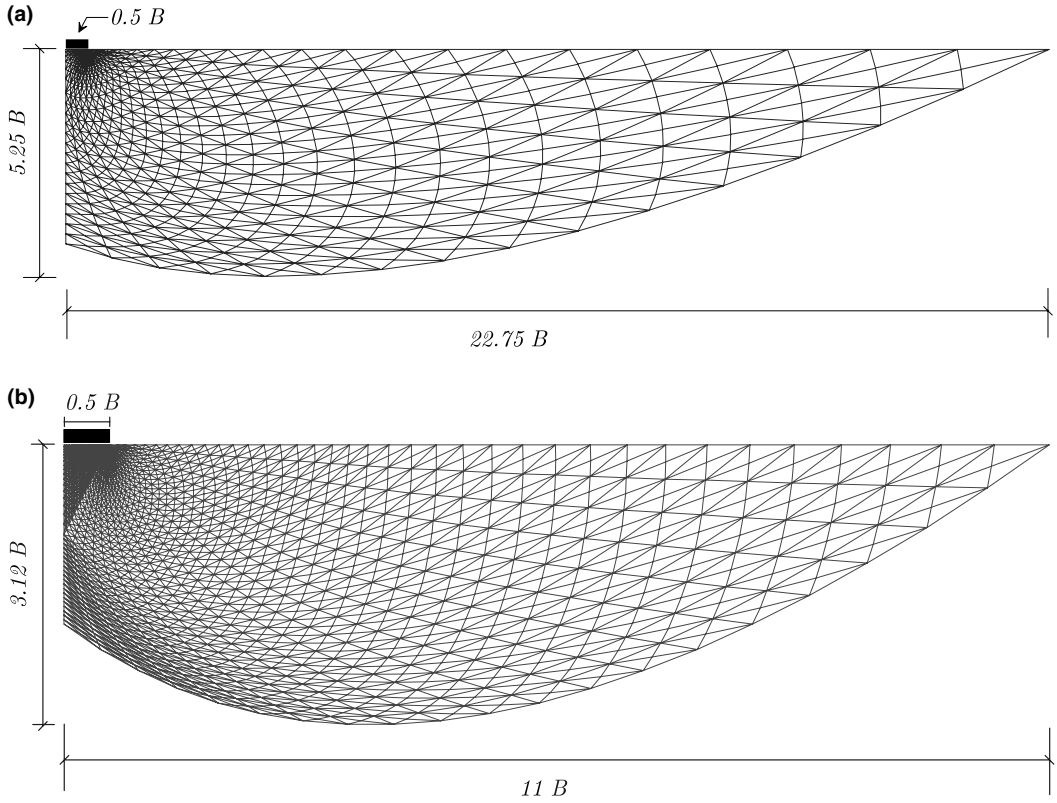


Fig. 8. (a) *1341 elements – 4023 nodes – 1980 discontinuities* (text just below the figure – the caption is below). Upper bound mesh for vertical loading – Weightless soil with $\phi = 45°$ (caption). (b) *4005 elements – 12015 nodes – 5952 discontinuities* (text just below the figure – the caption is below). Upper bound mesh for vertical loading – Ponderable soil with $\phi = 45°$ and $G = 3$ (caption).

Fig. 10 shows that the Meyerhof, Hansen and Vesić theories all underestimate the bearing capacity for a ponderable soil with $G = 0.5$. Hansen's predictions are the most conservative while Vesić's are the most accurate. Fig. 11 shows a similar plot for an example with $G = 3$. In this case, Vesić 's bearing capacities are slightly unconservative for$\phi$40°, Meyerhof's bearing capacities are the most accurate and Hansen's bearing capacities are again the most conservative. For the results shown in Figs. 10 and 11, the error measured by (22) varies between 3.31% and 20.92% for the Meyerhof theory, 3.36% and 22.79% for the Hansen theory, and −5.87%

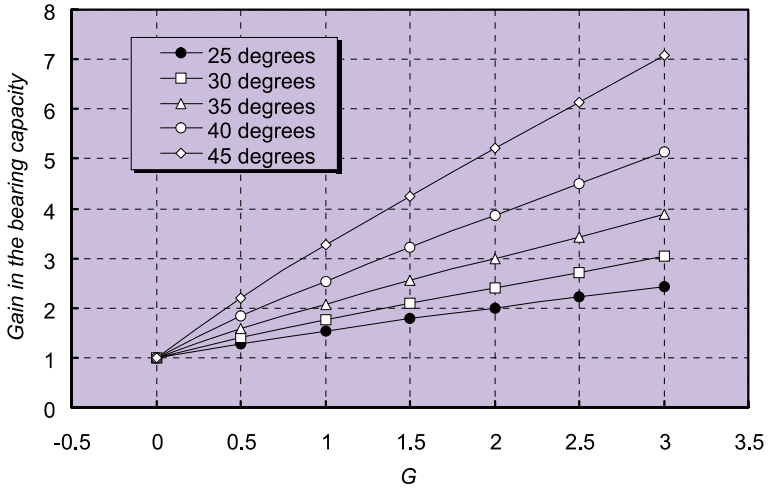


Fig. 9. Gain in the bearing capacity versus weight parameter $G$.

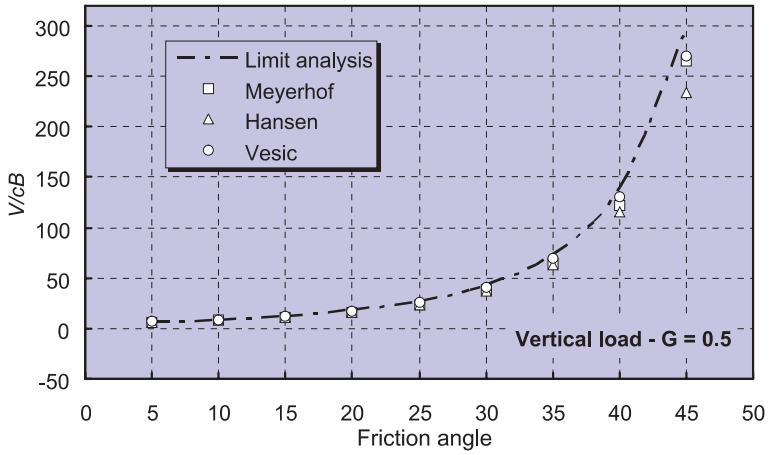


Fig. 10. Comparison between bearing capacity theories and numerical limit analysis for vertical loading with $G = 0.5$.

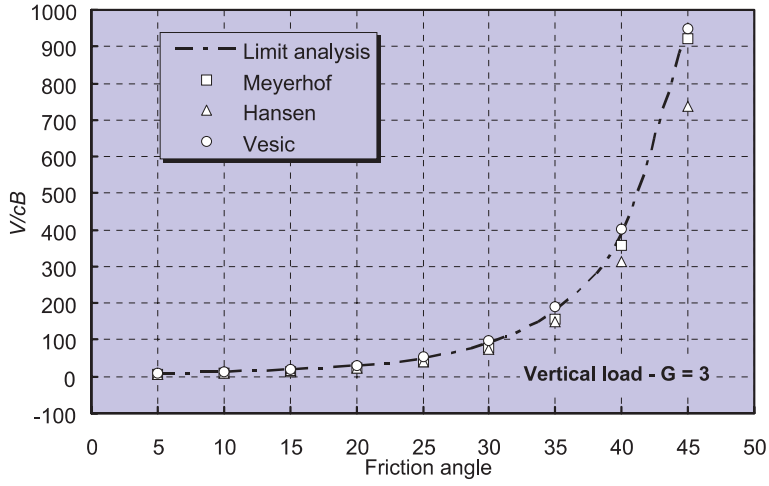


Fig. 11. Comparison between bearing capacity theories and numerical limit analysis for vertical loading with $G = 3$.

and −9.29% for the Vesić theory. Since the Meyerhof, Hansen, and Vesić theories all use identical expressions for $N_c$, the variations in their bearing capacity estimates are due solely to their different definitions of $N_\gamma$. The Meyerhof and Vesić $N_\gamma$ factors, although quite different in form, give similar predictions. The Hansen and Vesić $N_\gamma$ expressions, on the other hand, are identical in form but give different predictions due to their use of a different multiplicative factor. The results presented here suggest that the former is more conservative, whilst the latter is more accurate.

The correct value for $N_\gamma$ is unknown and has long been a subject of discussion in geotechnical research. Because of its importance, many $N_\gamma$ factors can be found in the literature. Some of these have been derived empirically by curve-fitting against experimental results, while others have been derived using limit equilibrium, slip-line, or upper bound rigid block methods. Not surprisingly, the predictions from various $N_\gamma$ expressions can differ widely. Recently, Bowles [3] noted that a literature survey gave $N_\gamma$ estimates ranging from 38 to 192 for a frictional soil with $\phi = 40°$. This unfortunate situation is further complicated by the fact that $N_\gamma$ is affected by the degree of footing roughness.

To gain a better understanding of the influence of self-weight on the bearing capacity, it is useful to compare the failure mechanisms and plastic zones for the weightless and ponderable cases. These are readily obtained from the velocity fields of the numerical upper bound method and are shown in Fig. 12 for a soil with $\phi = 45°$ and $G$ equal 0 and 3. Even though the size of the plastic zone is similar for the two cases, the self-weight clearly affects the mode of failure and gives much smaller surface deformations away from the footing. The failure mechanism for the weightless soil contains a rigid wedge directly beneath the

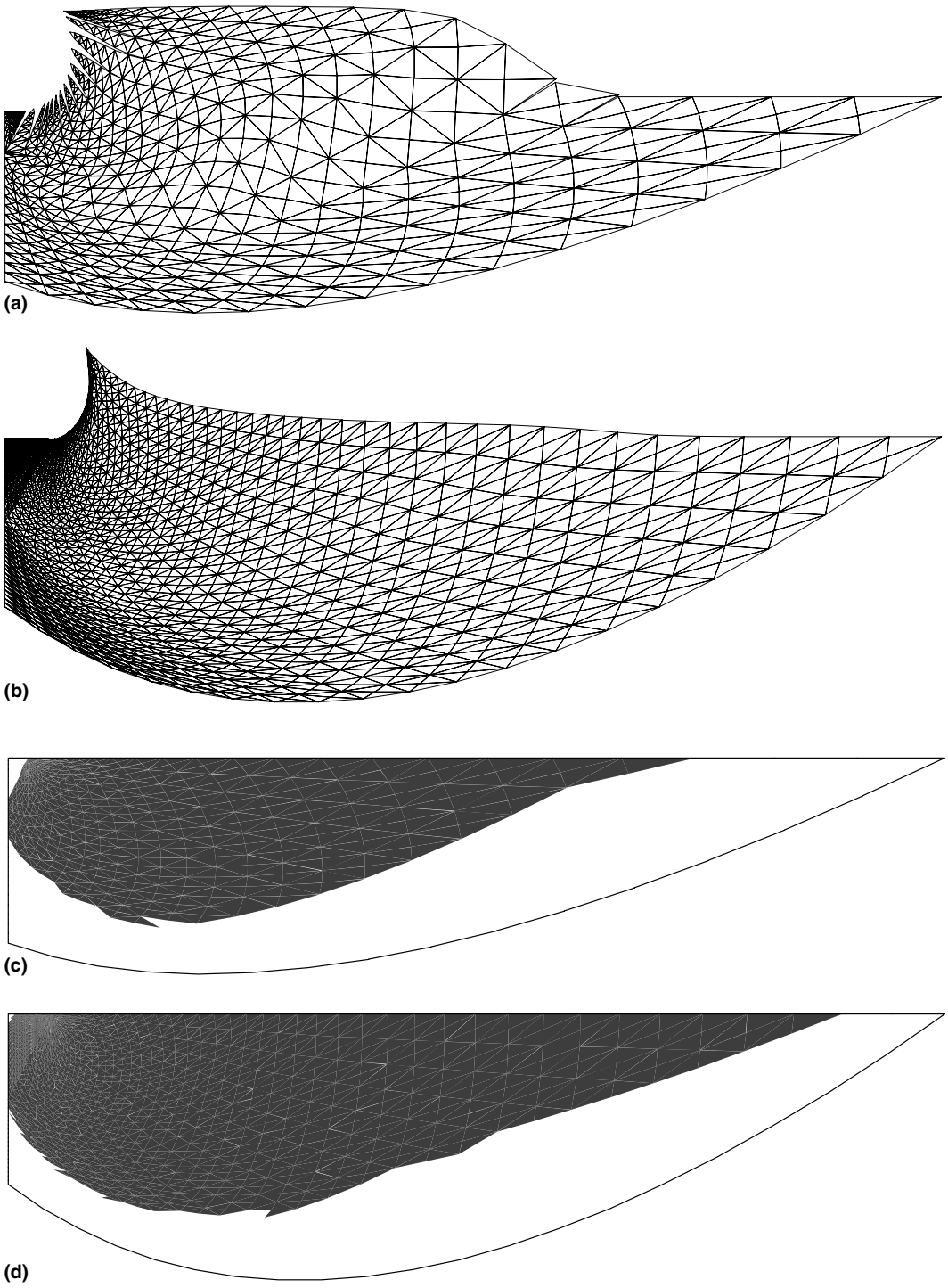


Fig. 12. (a) Deformed mesh for $\phi = 45°$ and $G = 0$. (b) Deformed mesh for $\phi = 45°$ and $G = 3$. (c) Plastic zone for $\phi = 45°$ and $G = 0$. (d) Plastic zone for $\phi = 45°$ and $G = 3$.

footing, and is similar to that assumed by Prandtl [17]. The corresponding velocity fields, shown in Fig. 13, confirm the dramatic difference in the modes of failure. For the weightless soil, the surface velocities adjacent to the footing have a constant magnitude and direction, indicating the presence of a passive wedge. No such mechanism is evident for the ponderable case, where the surface velocity magnitudes appear to decrease exponentially with increasing horizontal distance from the edge of the footing.

*6.2.2. The inclined loading case*

The inclinations factors derived by Meyerhof, Hansen and Vesić assume that failure occurs by general

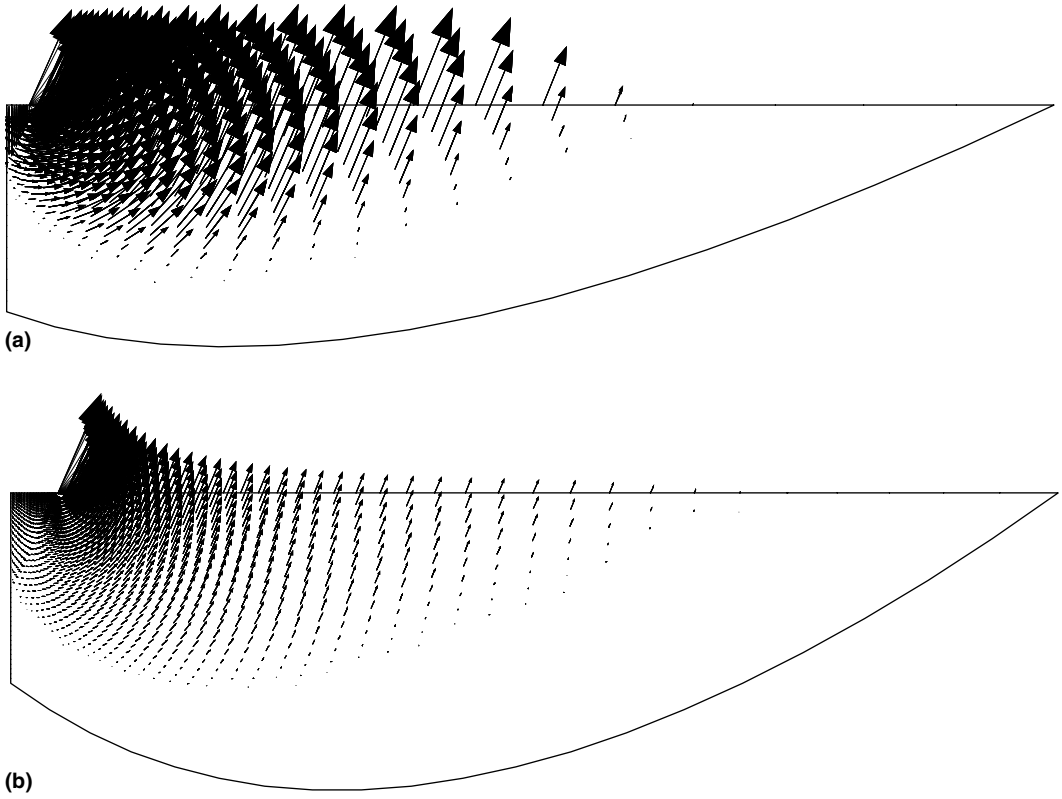


Fig. 13. (a) Velocity field for $\phi = 45°$ and $G = 0$. (b) Velocity field for $\phi = 45°$ and $G = 3$.

shearing and not by surface sliding. Since the results from the numerical upper bound analysis indicate which mode of failure actually prevails, we are thus able to select cases where direct comparison is possible. The weightless soil is considered first, followed by the ponderable case.

*6.2.2.1. Weightless soil.* Table 4 shows the numerical bearing capacities for a rough footing, under non-eccentric inclined loading, on a weightless cohesive-frictional soil. As expected, the bearing capacity decreases as the load inclination angle $\alpha$ increases. This decrease is substantial, even for small inclination angles, thus

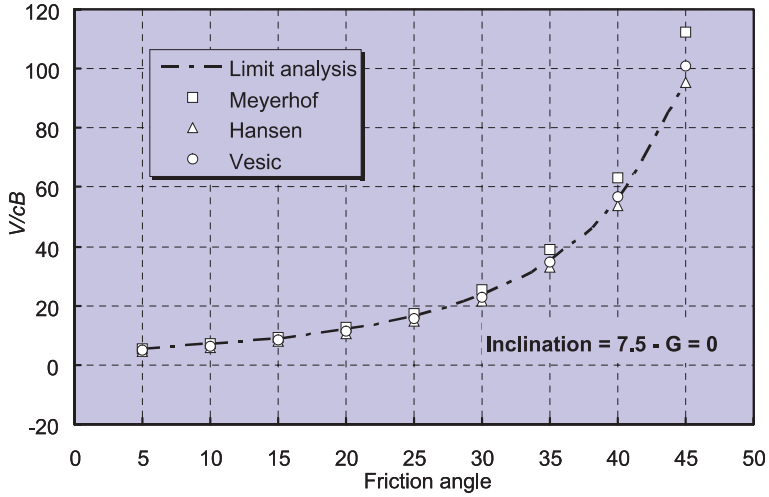


Fig. 14. Comparison between bearing capacity theories and numerical limit analysis for an inclination of 7.5°.

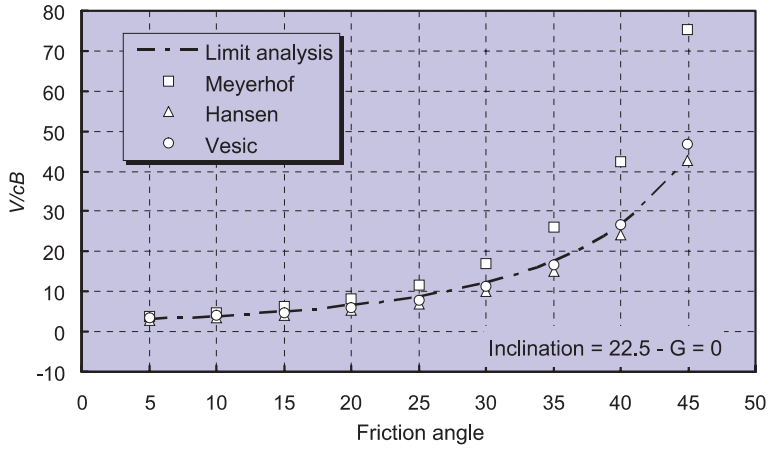


Fig. 15. Comparison between bearing capacity theories and numerical limit analysis for an inclination of 22.5°.

Table 5
Lower and upper bounds on the normalized bearing capacity pressure $V/cB$ for the ponderable soil with $G = 0.5$

| $\phi$ (°) | $\alpha = 0°$ | | | | $\alpha = 7.5°$ | | | |
|---|---|---|---|---|---|---|---|---|
| | LB | UB | Average | ±Error (%) | LB | UB | Average | ±Error (%) |
| 5 | 6.71 | 6.79 | 6.75 | 0.61 | 5.58 | 5.61 | 5.59 | 0.28 |
| 10 | 8.99 | 9.11 | 9.05 | 0.68 | 7.33 | 7.38 | 7.36 | 0.37 |
| 15 | 12.40 | 12.60 | 12.50 | 0.80 | 9.92 | 10.01 | 9.96 | 0.46 |
| 20 | 17.74 | 18.10 | 17.92 | 1.01 | 13.91 | 14.08 | 13.99 | 0.60 |
| 25 | 26.54 | 27.22 | 26.88 | 1.27 | 20.37 | 20.73 | 20.55 | 0.88 |
| 30 | 42.16 | 43.47 | 42.82 | 1.53 | 31.49 | 32.17 | 31.83 | 1.07 |
| 35 | 71.84 | 74.76 | 73.30 | 1.99 | 52.18 | 53.89 | 53.04 | 1.61 |
| 40 | 136.29 | 141.49 | 138.89 | 1.87 | 94.47 | 97.91 | 96.19 | 1.79 |
| 45 | 289.81 | 304.93 | 297.37 | 2.54 | 192.31 | 200.26 | 196.28 | 2.03 |
| | $\alpha = 15°$ | | | | $\alpha = 22.5°$ | | | |
| 5 | 4.30 | 4.35 | 4.33 | 0.52 | 3.04 | 3.06 | 3.05 | 0.30 |
| 10 | 5.57 | 5.63 | 5.60 | 0.55 | 3.90 | 3.94 | 3.92 | 0.53 |
| 15 | 7.41 | 7.49 | 7.45 | 0.59 | 5.13 | 5.19 | 5.16 | 0.56 |
| 20 | 10.17 | 10.31 | 10.24 | 0.68 | 6.94 | 7.04 | 6.99 | 0.66 |
| 25 | 14.55 | 14.76 | 14.65 | 0.72 | 9.73 | 9.92 | 9.83 | 0.98 |
| 30 | 21.87 | 22.24 | 22.05 | 0.85 | 14.26 | 14.65 | 14.45 | 1.35 |
| 35 | 34.95 | 35.84 | 35.39 | 1.26 | 22.11 | 22.74 | 22.43 | 1.41 |
| 40 | 60.72 | 62.52 | 61.62 | 1.46 | 36.86 | 38.10 | 37.48 | 1.66 |
| 45 | 117.28 | 122.53 | 119.90 | 2.19 | 67.56 | 70.37 | 68.97 | 2.04 |
| | $\alpha = 30°$ | | | | $\alpha = 45°$ | | | |
| 5 | 2.04 | 2.05 | 2.04 | 0.10 | 1.10 | 1.10 | 1.10 | 0.08 |
| 10 | 2.49 | 2.50 | 2.50 | 0.13 | 1.21 | 1.22 | 1.21 | 0.09 |
| 15 | 3.23 | 3.24 | 3.23 | 0.19 | 1.37 | 1.37 | 1.37 | 0.09 |
| 20 | 4.34 | 4.38 | 4.36 | 0.49 | 1.57 | 1.58 | 1.57 | 0.09 |
| 25 | 6.01 | 6.10 | 6.05 | 0.76 | 1.87 | 1.88 | 1.88 | 0.10 |
| 30 | 8.63 | 8.77 | 8.70 | 0.79 | 2.37 | 2.37 | 2.37 | 0.09 |
| 35 | 13.03 | 13.37 | 13.20 | 1.29 | 3.33 | 3.34 | 3.33 | 0.09 |
| 40 | 20.97 | 21.56 | 21.27 | 1.39 | 5.15 | 5.21 | 5.18 | 0.60 |
| 45 | 36.74 | 38.01 | 37.38 | 1.71 | 8.42 | 8.57 | 8.50 | 0.89 |

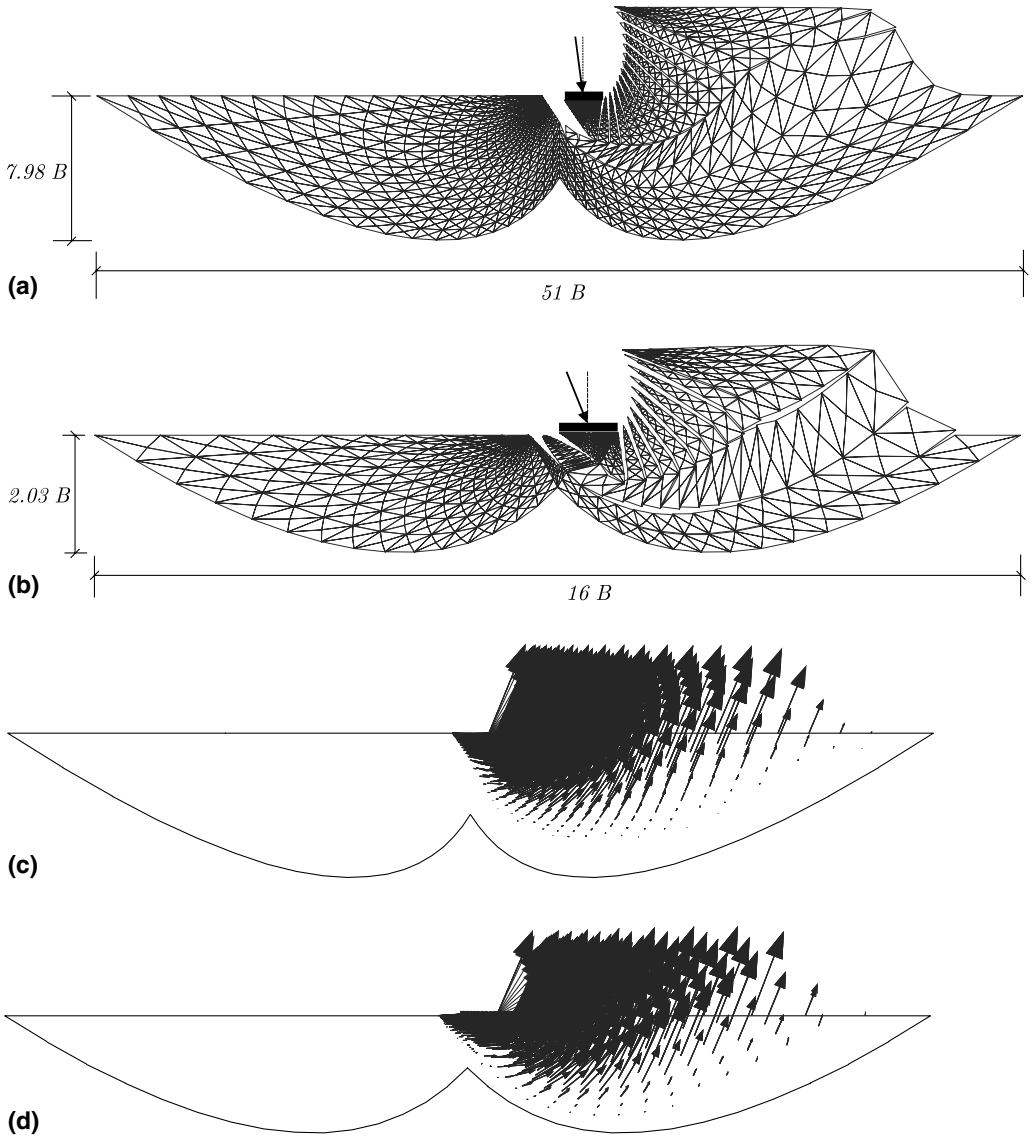


Fig. 16. (a) *3348 elements – 10044 nodes – 4973 discontinuities* (text just below the figure – the caption is below). Deformed mesh for a weightless soil with $\alpha = 7.5°$ and $\phi = 45°$ (caption). (b) *1702 elements – 5106 nodes – 2518 discontinuities* (text just below the figure – the caption is below). Deformed mesh for a weightless soil with $\alpha = 22.5°$ and $\phi = 45°$ (caption). (c) Velocity field for a weightless soil with $\alpha = 7.5°$ and $\phi = 45°$. (d) Velocity field for a weightless soil with $\alpha = 22.5°$ and $\phi = 45°$.

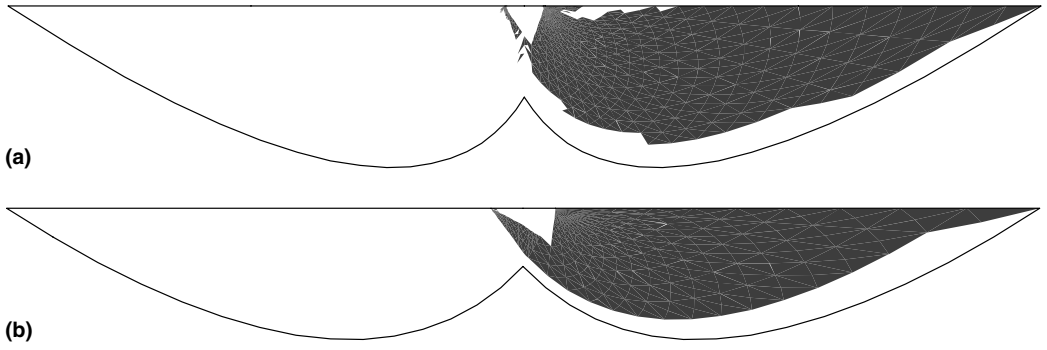


Fig. 17. (a) Plastic zone for a weightless soil with $\alpha = 7.5°$ and $\phi = 45°$. (b) Plastic zone for a weightless soil with $\alpha = 22.5°$ and $\phi = 45°$.

Table 6
Lower and upper bounds on the normalized bearing capacity pressure $V/cB$ for the ponderable soil with $G = 1$

| $\phi$ (°) | $\alpha$ = 0° | | | | $\alpha$ = 7.5° | | | |
|---|---|---|---|---|---|---|---|---|
| | LB | UB | Average | ±Error (%) | LB | UB | Average | ±Error (%) |
| 5 | 6.93 | 7.02 | 6.98 | 0.64 | 5.71 | 5.74 | 5.72 | 0.28 |
| 10 | 9.59 | 9.74 | 9.67 | 0.75 | 7.70 | 7.77 | 7.74 | 0.40 |
| 15 | 13.71 | 13.95 | 13.83 | 0.88 | 10.76 | 10.87 | 10.81 | 0.52 |
| 20 | 20.37 | 20.81 | 20.59 | 1.07 | 15.64 | 15.87 | 15.76 | 0.72 |
| 25 | 31.76 | 32.64 | 32.20 | 1.37 | 23.88 | 24.40 | 24.14 | 1.08 |
| 30 | 52.77 | 54.52 | 53.64 | 1.64 | 38.68 | 39.70 | 39.19 | 1.30 |
| 35 | 94.53 | 98.59 | 96.56 | 2.10 | 67.45 | 70.16 | 68.81 | 1.97 |
| 40 | 188.37 | 196.89 | 192.63 | 2.21 | 129.06 | 134.61 | 131.83 | 2.11 |
| 45 | 427.80 | 449.90 | 438.85 | 2.52 | 278.43 | 291.36 | 284.90 | 2.27 |
| | $\alpha$ = 15° | | | | $\alpha$ = 22.5° | | | |
| 5 | 4.36 | 4.41 | 4.38 | 0.57 | 3.04 | 3.06 | 3.05 | 0.31 |
| 10 | 5.75 | 5.82 | 5.78 | 0.61 | 3.95 | 3.99 | 3.97 | 0.59 |
| 15 | 7.83 | 7.94 | 7.89 | 0.70 | 5.28 | 5.35 | 5.32 | 0.65 |
| 20 | 11.11 | 11.28 | 11.20 | 0.78 | 7.33 | 7.45 | 7.39 | 0.80 |
| 25 | 16.49 | 16.77 | 16.63 | 0.85 | 10.61 | 10.87 | 10.74 | 1.22 |
| 30 | 25.91 | 26.44 | 26.17 | 1.01 | 16.19 | 16.73 | 16.46 | 1.65 |
| 35 | 43.57 | 44.86 | 44.22 | 1.46 | 26.34 | 27.29 | 26.81 | 1.78 |
| 40 | 79.95 | 82.70 | 81.33 | 1.69 | 46.40 | 48.26 | 47.33 | 1.96 |
| 45 | 164.27 | 172.44 | 168.35 | 2.43 | 90.57 | 94.55 | 92.56 | 2.15 |
| | $\alpha$ = 30° | | | | $\alpha$ = 45° | | | |
| 5 | 2.04 | 2.05 | 2.04 | 0.12 | 1.10 | 1.10 | 1.10 | 0.08 |
| 10 | 2.49 | 2.50 | 2.50 | 0.13 | 1.21 | 1.22 | 1.21 | 0.08 |
| 15 | 3.23 | 3.24 | 3.24 | 0.15 | 1.37 | 1.37 | 1.37 | 0.09 |
| 20 | 4.42 | 4.47 | 4.44 | 0.52 | 1.57 | 1.58 | 1.57 | 0.10 |
| 25 | 6.28 | 6.39 | 6.33 | 0.89 | 1.87 | 1.88 | 1.88 | 0.11 |
| 30 | 9.34 | 9.51 | 9.42 | 0.94 | 2.37 | 2.37 | 2.37 | 0.10 |
| 35 | 14.72 | 15.18 | 14.95 | 1.55 | 3.34 | 3.34 | 3.34 | 0.06 |
| 40 | 24.81 | 25.80 | 25.31 | 1.95 | 5.35 | 5.42 | 5.38 | 0.70 |
| 45 | 46.55 | 48.42 | 47.49 | 1.97 | 9.20 | 9.40 | 9.30 | 1.06 |

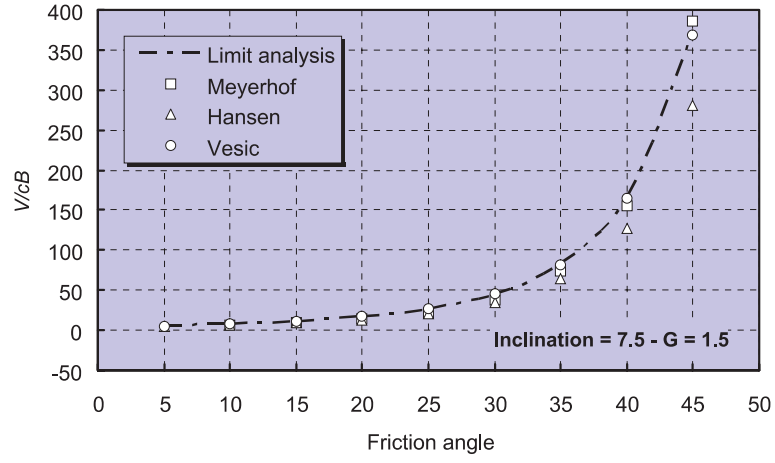


Fig. 18. Comparison between bearing capacity theories and numerical limit analysis for $\alpha = 7.5°$ and $G = 1.5$.

Table 7
Lower and upper bounds on the normalized bearing capacity pressure $VlcB$ for the ponderable soil with $G = 1.5$

| $\phi$ (°) | $\alpha$ = 0° | | | | $\alpha$ = 7.5° | | | |
|---|---|---|---|---|---|---|---|---|
| | LB | UB | Average | ±Error (%) | LB | UB | Average | ±Error (%) |
| 5 | 7.14 | 7.24 | 7.19 | 0.71 | 5.83 | 5.87 | 5.85 | 0.30 |
| 10 | 10.14 | 10.31 | 10.23 | 0.83 | 8.06 | 8.13 | 8.10 | 0.42 |
| 15 | 14.89 | 15.18 | 15.03 | 0.97 | 11.55 | 11.68 | 11.61 | 0.55 |
| 20 | 22.76 | 23.29 | 23.02 | 1.15 | 17.27 | 17.55 | 17.41 | 0.80 |
| 25 | 36.57 | 37.62 | 37.10 | 1.41 | 27.19 | 27.86 | 27.52 | 1.22 |
| 30 | 62.51 | 64.77 | 63.64 | 1.77 | 45.46 | 46.81 | 46.14 | 1.46 |
| 35 | 115.54 | 120.84 | 118.19 | 2.25 | 81.91 | 85.56 | 83.73 | 2.18 |
| 40 | 237.25 | 249.27 | 243.26 | 2.47 | 161.94 | 169.68 | 165.81 | 2.34 |
| 45 | 556.88 | 587.25 | 572.06 | 2.65 | 360.79 | 378.80 | 369.80 | 2.44 |
| | $\alpha$ = 15° | | | | $\alpha$ = 22.5° | | | |
| 5 | 4.39 | 4.46 | 4.43 | 0.86 | 3.05 | 3.07 | 3.06 | 0.27 |
| 10 | 5.91 | 5.99 | 5.95 | 0.67 | 3.99 | 4.04 | 4.01 | 0.58 |
| 15 | 8.23 | 8.36 | 8.30 | 0.78 | 5.42 | 5.50 | 5.46 | 0.71 |
| 20 | 11.98 | 12.19 | 12.09 | 0.88 | 7.68 | 7.82 | 7.75 | 0.94 |
| 25 | 18.32 | 18.67 | 18.50 | 0.96 | 11.42 | 11.76 | 11.59 | 1.43 |
| 30 | 29.73 | 30.39 | 30.06 | 1.10 | 17.99 | 18.69 | 18.34 | 1.91 |
| 35 | 51.77 | 53.43 | 52.60 | 1.58 | 30.32 | 31.60 | 30.96 | 2.07 |
| 40 | 98.37 | 101.99 | 100.18 | 1.80 | 55.52 | 58.01 | 56.77 | 2.20 |
| 45 | 209.52 | 220.64 | 215.08 | 2.59 | 112.64 | 117.98 | 115.31 | 2.32 |
| | $\alpha$ = 30° | | | | $\alpha$ = 45° | | | |
| 5 | 2.04 | 2.05 | 2.04 | 0.11 | 1.10 | 1.10 | 1.10 | 0.07 |
| 10 | 2.49 | 2.50 | 2.50 | 0.15 | 1.21 | 1.22 | 1.22 | 0.08 |
| 15 | 3.23 | 3.24 | 3.24 | 0.18 | 1.37 | 1.37 | 1.37 | 0.10 |
| 20 | 4.49 | 4.53 | 4.51 | 0.53 | 1.57 | 1.58 | 1.57 | 0.11 |
| 25 | 6.51 | 6.65 | 6.58 | 1.01 | 1.87 | 1.88 | 1.88 | 0.12 |
| 30 | 9.93 | 10.19 | 10.06 | 1.29 | 2.37 | 2.37 | 2.37 | 0.11 |
| 35 | 16.29 | 16.87 | 16.58 | 1.77 | 3.34 | 3.34 | 3.34 | 0.09 |
| 40 | 28.76 | 29.82 | 29.29 | 1.81 | 5.51 | 5.59 | 5.55 | 0.75 |
| 45 | 55.92 | 58.39 | 57.16 | 2.16 | 9.91 | 10.15 | 10.03 | 1.21 |

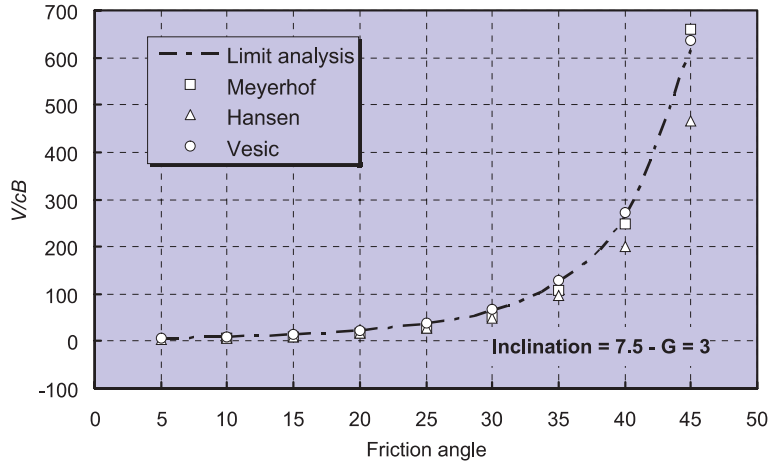


Fig. 19. Comparison between bearing capacity theories and numerical limit analysis for $\alpha = 7.5°$ and $G = 3$.

Table 8
Lower and upper bounds on the normalized bearing capacity pressure $V/cB$ for the ponderable soil with $G = 2$

| $\phi$ (°) | $\alpha = 0°$ | | | | $\alpha = 7.5°$ | | | |
|---|---|---|---|---|---|---|---|---|
| | LB | UB | Average | ±Error (%) | LB | UB | Average | ±Error (%) |
| 5 | 7.33 | 7.45 | 7.39 | 0.78 | 5.95 | 5.99 | 5.97 | 0.29 |
| 10 | 10.65 | 10.85 | 10.75 | 0.93 | 8.40 | 8.47 | 8.44 | 0.45 |
| 15 | 15.99 | 16.33 | 16.16 | 1.06 | 12.30 | 12.45 | 12.37 | 0.60 |
| 20 | 25.00 | 25.62 | 25.31 | 1.24 | 18.83 | 19.17 | 19.00 | 0.89 |
| 25 | 41.08 | 42.34 | 41.71 | 1.52 | 30.35 | 31.17 | 30.76 | 1.33 |
| 30 | 71.80 | 74.55 | 73.18 | 1.87 | 51.98 | 53.64 | 52.81 | 1.57 |
| 35 | 135.60 | 142.25 | 138.93 | 2.39 | 95.85 | 100.41 | 98.13 | 2.33 |
| 40 | 284.35 | 299.99 | 292.17 | 2.68 | 193.88 | 203.79 | 198.84 | 2.49 |
| 45 | 682.67 | 721.59 | 702.13 | 2.77 | 441.29 | 464.36 | 452.82 | 2.55 |
| | $\alpha = 15°$ | | | | $\alpha = 22.5°$ | | | |
| 5 | 4.46 | 4.52 | 4.49 | 0.64 | 3.05 | 3.07 | 3.06 | 0.27 |
| 10 | 6.07 | 6.16 | 6.11 | 0.74 | 4.03 | 4.07 | 4.05 | 0.57 |
| 15 | 8.61 | 8.76 | 8.68 | 0.87 | 5.54 | 5.63 | 5.59 | 0.78 |
| 20 | 12.81 | 13.06 | 12.93 | 0.98 | 8.01 | 8.18 | 8.09 | 1.05 |
| 25 | 20.07 | 20.50 | 20.28 | 1.06 | 12.20 | 12.59 | 12.39 | 1.60 |
| 30 | 33.40 | 34.23 | 33.81 | 1.23 | 19.71 | 20.58 | 20.14 | 2.16 |
| 35 | 59.72 | 61.78 | 60.75 | 1.70 | 34.18 | 35.80 | 34.99 | 2.31 |
| 40 | 116.36 | 120.85 | 118.61 | 1.89 | 64.39 | 67.55 | 65.97 | 2.40 |
| 45 | 253.81 | 267.75 | 260.78 | 2.67 | 134.18 | 141.10 | 137.64 | 2.51 |
| | $\alpha = 30°$ | | | | $\alpha = 45°$ | | | |
| 5 | 2.04 | 2.05 | 2.04 | 0.10 | 1.10 | 1.10 | 1.10 | 0.10 |
| 10 | 2.49 | 2.50 | 2.50 | 0.17 | 1.21 | 1.22 | 1.21 | 0.09 |
| 15 | 3.23 | 3.25 | 3.24 | 0.23 | 1.37 | 1.37 | 1.37 | 0.11 |
| 20 | 4.54 | 4.59 | 4.56 | 0.51 | 1.57 | 1.58 | 1.57 | 0.12 |
| 25 | 6.73 | 6.88 | 6.80 | 1.11 | 1.87 | 1.88 | 1.88 | 0.12 |
| 30 | 10.58 | 10.83 | 10.70 | 1.16 | 2.37 | 2.37 | 2.37 | 0.13 |
| 35 | 17.79 | 18.49 | 18.14 | 1.94 | 3.34 | 3.34 | 3.34 | 0.12 |
| 40 | 32.41 | 33.72 | 33.07 | 1.99 | 5.65 | 5.74 | 5.69 | 0.81 |
| 45 | 65.05 | 68.13 | 66.59 | 2.32 | 10.57 | 10.86 | 10.71 | 1.34 |

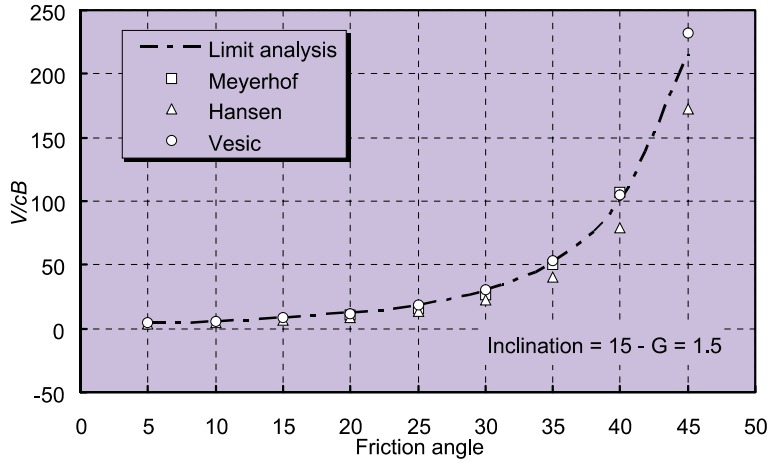


Fig. 20. Comparison between bearing capacity theories and numerical limit analysis for $\alpha = 15°$ and $G = 1.5$.

Table 9
Lower and upper bounds on the normalized bearing capacity pressure $V/cB$ for the ponderable soil with $G = 2.5$

| $\phi$ (°) | $\alpha$ = 0° | | | | $\alpha$ = 7.5° | | | |
|---|---|---|---|---|---|---|---|---|
| | LB | UB | Average | ±Error (%) | LB | UB | Average | ±Error (%) |
| 5 | 7.51 | 7.64 | 7.58 | 0.85 | 6.07 | 6.10 | 6.09 | 0.29 |
| 10 | 11.14 | 11.36 | 11.25 | 1.00 | 8.72 | 8.80 | 8.76 | 0.50 |
| 15 | 17.01 | 17.42 | 17.22 | 1.19 | 13.02 | 13.20 | 13.11 | 0.67 |
| 20 | 27.10 | 27.85 | 27.48 | 1.37 | 20.33 | 20.73 | 20.53 | 0.96 |
| 25 | 45.43 | 46.88 | 46.16 | 1.57 | 33.42 | 34.38 | 33.90 | 1.41 |
| 30 | 80.82 | 84.04 | 82.43 | 1.95 | 58.32 | 60.27 | 59.30 | 1.65 |
| 35 | 155.26 | 163.13 | 159.20 | 2.47 | 109.48 | 114.92 | 112.20 | 2.43 |
| 40 | 330.58 | 349.69 | 340.14 | 2.81 | 225.20 | 237.23 | 231.21 | 2.60 |
| 45 | 806.15 | 848.50 | 827.33 | 2.56 | 520.54 | 548.63 | 534.58 | 2.63 |
| | $\alpha$ = 15° | | | | $\alpha$ = 22.5° | | | |
| 5 | 4.50 | 4.57 | 4.54 | 0.68 | 3.06 | 3.07 | 3.06 | 0.23 |
| 10 | 6.21 | 6.31 | 6.26 | 0.78 | 4.06 | 4.10 | 4.08 | 0.56 |
| 15 | 8.97 | 9.14 | 9.05 | 0.93 | 5.66 | 5.75 | 5.70 | 0.85 |
| 20 | 13.59 | 13.89 | 13.74 | 1.11 | 8.31 | 8.51 | 8.41 | 1.16 |
| 25 | 21.77 | 22.27 | 22.02 | 1.15 | 12.93 | 13.39 | 13.16 | 1.77 |
| 30 | 36.98 | 37.98 | 37.48 | 1.33 | 21.39 | 22.41 | 21.90 | 2.33 |
| 35 | 67.51 | 70.00 | 68.75 | 1.81 | 37.94 | 39.91 | 38.93 | 2.53 |
| 40 | 134.04 | 139.47 | 136.76 | 1.99 | 73.05 | 76.96 | 75.01 | 2.61 |
| 45 | 297.59 | 314.30 | 305.95 | 2.73 | 155.45 | 163.98 | 159.72 | 2.67 |
| | $\alpha$ = 30° | | | | $\alpha$ = 45° | | | |
| 5 | 2.04 | 2.05 | 2.04 | 0.11 | 1.10 | 1.10 | 1.10 | 0.08 |
| 10 | 2.49 | 2.50 | 2.50 | 0.18 | 1.21 | 1.22 | 1.21 | 0.10 |
| 15 | 3.23 | 3.25 | 3.24 | 0.26 | 1.37 | 1.37 | 1.37 | 0.10 |
| 20 | 4.58 | 4.63 | 4.60 | 0.48 | 1.57 | 1.58 | 1.57 | 0.14 |
| 25 | 6.92 | 7.09 | 7.00 | 1.24 | 1.87 | 1.88 | 1.88 | 0.14 |
| 30 | 11.15 | 11.43 | 11.29 | 1.26 | 2.37 | 2.37 | 2.37 | 0.15 |
| 35 | 19.23 | 20.06 | 19.64 | 2.11 | 3.34 | 3.34 | 3.34 | 0.15 |
| 40 | 35.95 | 37.55 | 36.75 | 2.17 | 5.76 | 5.86 | 5.81 | 0.84 |
| 45 | 74.03 | 77.73 | 75.88 | 2.44 | 11.20 | 11.53 | 11.36 | 1.44 |

indicating the importance of accounting for inclined loading in design. For example, a footing on a soil with $\phi = 45°$ and $\alpha = 15°$ has an ultimate bearing capacity which is roughly 50% less than that of a comparable footing under vertical loading. From Table 4 we observe that, for an inclined load on a weightless soil, the algorithms employed give very sharp bounds whose errors (21) do not exceed ±2.68%.

Except for the case of $\alpha = 7.5°$ and $\phi = 5°$, these results show that Meyerhof's predictions are always on the unsafe side for a weightless soil (see Figs. 14 and 15). Indeed, for a load inclination of 30° and a soil with

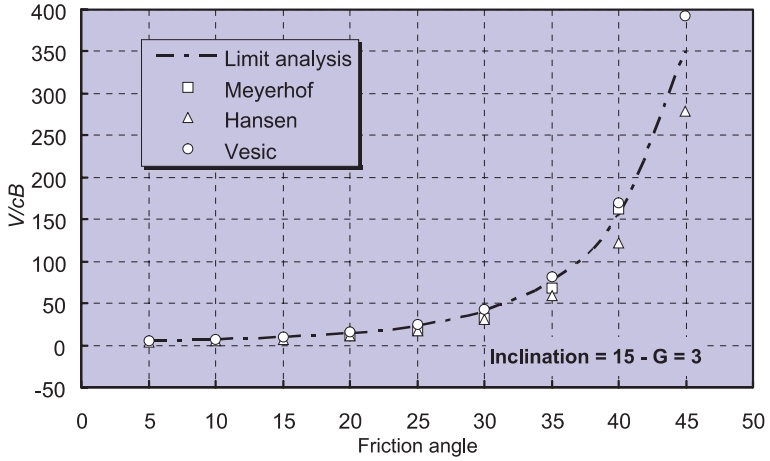


Fig. 21. Comparison between bearing capacity theories and numerical limit analysis for $\alpha = 15°$ and $G = 3$.

Table 10
Lower and upper bounds on the normalized bearing capacity pressure $V/cB$ for the ponderable soil with $G = 3$

| $\phi$ (°) | $\alpha = 0°$ | | | | $\alpha = 7.5°$ | | | |
|---|---|---|---|---|---|---|---|---|
| | LB | UB | Average | ±Error (%) | LB | UB | Average | ±Error (%) |
| 5 | 7.70 | 7.83 | 7.77 | 0.85 | 6.18 | 6.22 | 6.20 | 0.32 |
| 10 | 11.60 | 11.85 | 11.72 | 1.08 | 9.02 | 9.13 | 9.08 | 0.56 |
| 15 | 18.08 | 18.47 | 18.27 | 1.08 | 13.72 | 13.92 | 13.82 | 0.73 |
| 20 | 29.30 | 30.01 | 29.65 | 1.19 | 21.74 | 22.24 | 21.99 | 1.14 |
| 25 | 49.94 | 51.30 | 50.62 | 1.34 | 36.31 | 37.50 | 36.90 | 1.62 |
| 30 | 90.58 | 93.32 | 91.95 | 1.49 | 64.31 | 66.77 | 65.54 | 1.88 |
| 35 | 177.17 | 183.63 | 180.40 | 1.79 | 122.84 | 129.19 | 126.02 | 2.52 |
| 40 | 381.28 | 398.61 | 389.94 | 2.22 | 256.07 | 270.21 | 263.14 | 2.69 |
| 45 | 928.63 | 978.64 | 953.64 | 2.62 | 598.84 | 632.08 | 615.46 | 2.70 |
| | $\alpha = 15°$ | | | | $\alpha = 22.5°$ | | | |
| 5 | 4.55 | 4.61 | 4.58 | 0.71 | 3.06 | 3.07 | 3.07 | 0.21 |
| 10 | 6.35 | 6.46 | 6.41 | 0.85 | 4.09 | 4.13 | 4.11 | 0.53 |
| 15 | 9.31 | 9.50 | 9.41 | 1.02 | 5.76 | 5.86 | 5.81 | 0.90 |
| 20 | 14.36 | 14.71 | 14.53 | 1.19 | 8.60 | 8.82 | 8.71 | 1.27 |
| 25 | 23.41 | 23.97 | 23.69 | 1.20 | 13.64 | 14.17 | 13.91 | 1.91 |
| 30 | 40.51 | 41.67 | 41.09 | 1.41 | 23.04 | 24.20 | 23.62 | 2.46 |
| 35 | 75.17 | 78.12 | 76.65 | 1.93 | 41.64 | 43.96 | 42.80 | 2.71 |
| 40 | 151.63 | 157.92 | 154.78 | 2.03 | 81.65 | 86.27 | 83.96 | 2.75 |
| 45 | 340.81 | 360.53 | 350.67 | 2.81 | 176.79 | 186.68 | 181.74 | 2.72 |
| | $\alpha = 30°$ | | | | $\alpha = 45°$ | | | |
| 5 | 2.04 | 2.05 | 2.04 | 0.11 | 1.10 | 1.10 | 1.10 | 0.09 |
| 10 | 2.49 | 2.50 | 2.50 | 0.20 | 1.21 | 1.22 | 1.21 | 0.10 |
| 15 | 3.23 | 3.25 | 3.24 | 0.31 | 1.37 | 1.37 | 1.37 | 0.12 |
| 20 | 4.62 | 4.66 | 4.64 | 0.47 | 1.57 | 1.58 | 1.57 | 0.13 |
| 25 | 7.10 | 7.29 | 7.19 | 1.31 | 1.87 | 1.88 | 1.88 | 0.15 |
| 30 | 11.69 | 12.01 | 11.85 | 1.36 | 2.37 | 2.37 | 2.37 | 0.16 |
| 35 | 20.64 | 21.59 | 21.12 | 2.25 | 3.34 | 3.35 | 3.34 | 0.18 |
| 40 | 39.46 | 41.31 | 40.39 | 2.29 | 5.86 | 5.96 | 5.91 | 0.86 |
| 45 | 82.97 | 87.24 | 85.11 | 2.51 | 11.78 | 12.17 | 11.98 | 1.60 |

$\phi = 45°$, the ultimate load predicted by Meyerhof is more than twice the average numerical limit load (whose bounding error (21) is just ±2.56%). For a given friction angle, this overestimation increases as the load inclination increases. This suggests that the Meyerhof expressions for $i_q$ and $i_c$ should be used with care when $G$ is small. Vesić 's predictions are reasonably close to the averaged upper and lower bounds over a wide range of friction angles and load inclinations, though they are unconservative for cases where $\phi$>45°. The Hansen theory gives results which are always conservative, with a maximum error of −20% with respect to the average

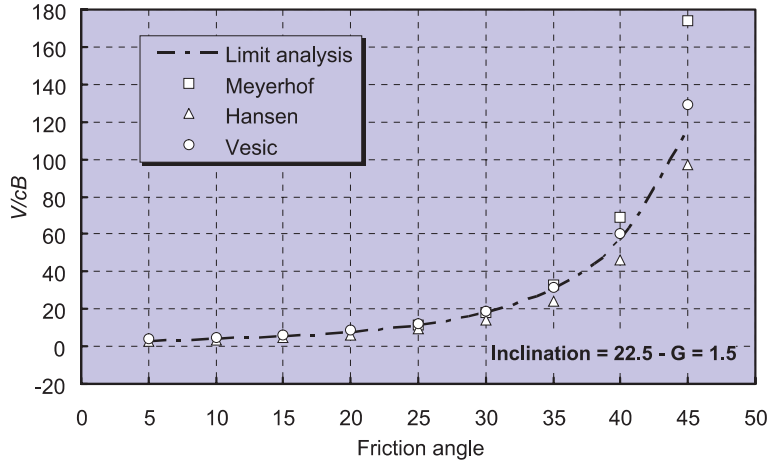


Fig. 22. Comparison between bearing capacity theories and numerical limit analysis for $\alpha = 22.5°$ and $G = 1.5$.

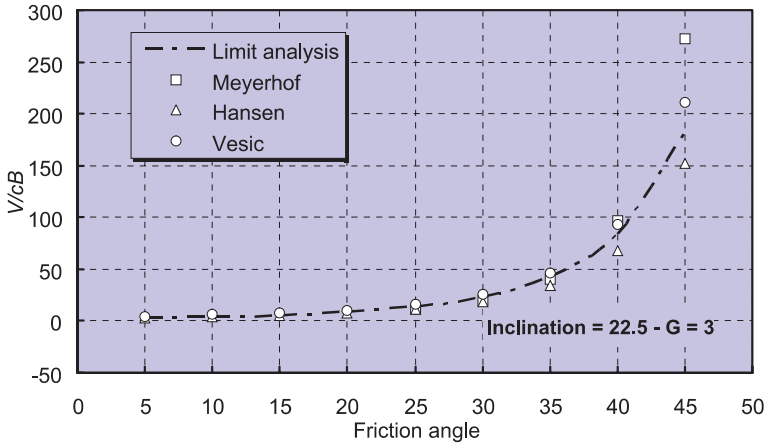


Fig. 23. Comparison between bearing capacity theories and numerical limit analysis for $\alpha = 22.5°$ and $G = 3$.

numerical limit load. Although Hansen's predictions are close to the average limit load, especially for high friction angles, their accuracy depends on the values chosen for the exponents $\delta_1$ and $\delta_2$ (Table 2). Adopting $\delta_1 = \delta_2 = 5$, as suggested by Hansen, seems to give good estimates of the ultimate load, at least for the case of a weightless soil.

Fig. 16 shows that the failure mechanism is asymmetrical and confined to one side of the footing for all values of the inclination angle when $\phi = 45°$. Furthermore, the mechanism seems to be composed of three different zones and similar to the one assumed by Meyerhof and Hansen. From the mesh deformation and plastic zone plots, shown in Figs. 16 and 17, we can observe a rigid wedge underneath the footing and a passive shearing zone adjacent to it. Although the shape of the rigid wedge changes significantly with the inclination of the load, the direction of the surface velocities appears to be more or less constant. As expected, the extent of the plastic zone decreases as the inclination of the load increases.

*6.2.2.2. Ponderable soil.* As in the case of vertical loading, self-weight increases the bearing capacity of a footing subjected to an inclined load. This influence diminishes as the inclination angle increases, however, and is zero once the load is purely horizontal (see Tables 5–10). Figs. 18–23 compare the predictions of the Meyerhof, Hansen and Vesić theories with the upper and lower bound averages for a variety of cases. For a load inclination angle of 7.5°, the Meyerhof predictions are conservative for all values of $G$, provided $5° \leqslant \phi < 45°$. At larger load inclination angles, however, Meyerhof's predictions become increasingly unsafe, especially for high friction angles. Indeed, the Meyerhof estimates are unconservative for all cases where $\alpha = 30°$ or $\alpha = 22.5°$ and $G \leqslant 1.5$. One drawback of this bearing capacity theory is that its expression for $i_\gamma$ does not permit the inclination angle to be greater than the friction angle, even if failure is caused by general shear. As indicated in Tables 4–10, this prevents many practical cases from being analysed. The Vesić formulas yield conservative bearing capacities only for low inclination angles ($\leqslant 7.5°$) and moderate values of $G$ ($\leqslant$ 1.5). For these moderate $G$ values, the predictions become progressively more unconservative as the inclination angle increases. For higher values of $G$ (>1.5), Vesić 's estimates exceed the average of the numerical bounds, regardless of the load inclination and the friction angle. Except for cases where $\alpha \geq 30°$, or where the failure mechanism swaps from sliding to general shearing, the Hansen theory yields predictions which are conservative.

Perhaps the most surprising behaviour revealed by the upper bound analysis is that, for a ponderable soil, the failure mechanism can be a two-sided one, depending on the weight parameter $G$, the load inclination angle $\alpha$, and the friction angle $\phi$. This is shown in Figs. 24 and 25 for $\phi = 45°$, $G = 3$ and $\alpha =$ (7.5°,22.5°). This suggests that the one-sided mechanisms adopted by Meyerhof, Hansen and Vesić are physically incorrect, especially for cases where $G$ is large. As in the example with purely vertical loading, a rigid wedge is formed directly underneath the footing at failure. For fixed values of $G$ and $\phi$, the size of this wedge increases with increasing $\alpha$.

## 7. Conclusions

The bearing capacity of strip footing, subjected to a non-eccentric inclined load and resting on a ponderable cohesive-frictional soil, has been investigated. The numerical formulations of the bound theorems, using a finite element discretization and nonlinear programming as described by Lyamin and Sloan [12,13], proved to be a practical, efficient, and accurate tool for this purpose. The calculated bounds are accurate to 6%, so that their average can be used with an implied maximum

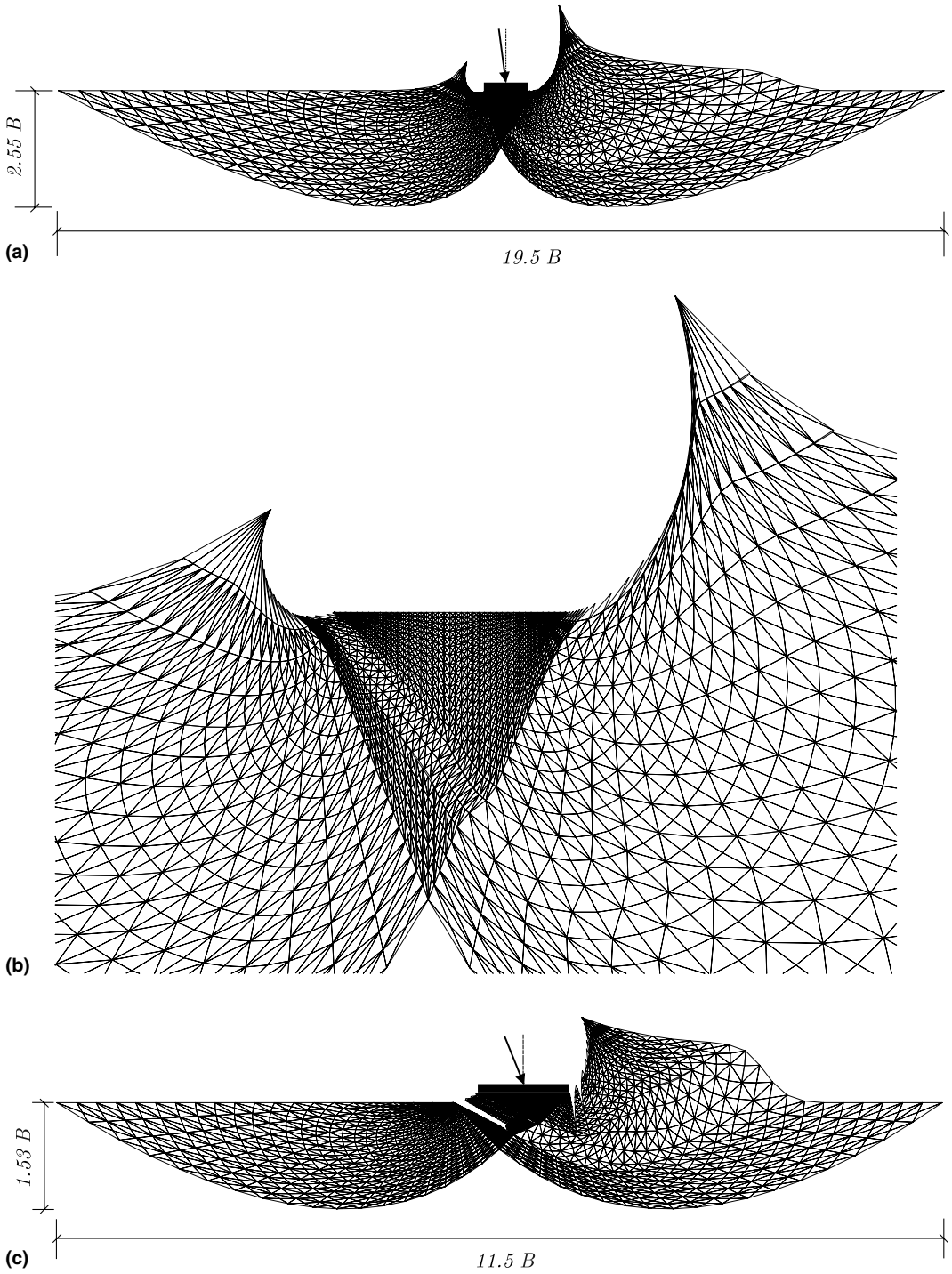


Fig. 24. (a) *6160 elements – 18480 nodes – 9180 discontinuities* (text just below the figure – the caption is below). Deformed mesh for $\alpha = 7.5°$, $\phi = 45°$ and $G = 3$ (caption). (b) Deformed mesh near footing for $\alpha = 7.5°$, $\phi = 45°$ and $G = 3$ (caption). (c) *698 elements – 17094 nodes – 8490 discontinuities* (text just below the figure – the caption is below). Deformed mesh for $\alpha = 22.5°$, $\phi = 45°$ and $G = 3$ (caption). (d) Velocity field for $\alpha = 7.5°$, $\phi = 45°$ and $G = 3$. (e) Velocity field for $\alpha = 22.5°$, $\phi = 45°$ and $G = 3$.

error of just ±3%. Comparing the new numerical solutions with the predictions of Meyerhof, Hansen and Vesić showed that some of these theories do not always provide conservative results and should therefore be applied with caution. The biggest discrepancies occur for cases where the friction or load inclination angle is large, and may exceed 50%. The study shows that the Meyerhof inclination factors are deficient for non-eccentric inclined loading and that the Vesić expression for $N_\gamma$ slightly overestimates the influence of self-weight on

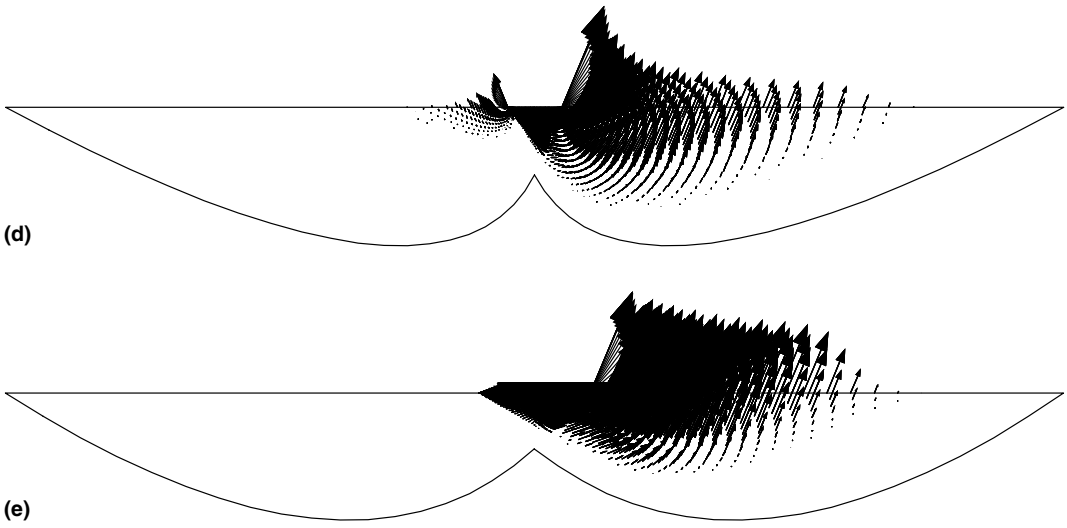


Fig. 24 (*continued*)

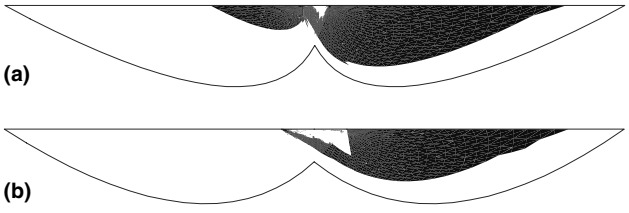


Fig. 25. (a) Plastic zone for $\alpha = 7.5°$, $\phi = 45°$ and $G = 3$. (b) Plastic zone for $\alpha = 22.5°$, $\phi = 45°$ and $G = 3$.

the bearing capacity. The upper bound analyses indicate that the failure mechanism for a vertically loaded footing on a ponderable soil is clearly different to the Prandtl–Hill one, which has been widely used in previous theoretical studies. Furthermore, for non-eccentric inclined loadings, the failure mechanism can be two-sided. All these remarks highlight the difficulty of obtaining analytical bearing capacity solutions for inclined loading of a footing on a ponderable cohesive-frictional soil.

## References

[1] Abbo AJ, Sloan SW. A smooth hyperbolic approximation to the Mohr–Coulomb yield criterion. Comput Struct 1995;54(3):427–41.
[2] Booker JR. Applications of theories of plasticity to cohesive frictional soils. PhD thesis, Sydney University; 1969.
[3] Bowles JE. Foundation analysis and design. New York: McGraw-Hill; 1996.
[4] Caquot A, Kérisel J. Sur le terme de surface dans le calcul des fondations en milieu pulvérulents. In: Proceedings of the third international conference on soil mechanics and foundation engineering, Zürich; 1953. p. 336–7.
[5] Cox AD. Axially symmetric plastic deformation of soils – II – indentation of ponderable soils. Int J Mech Sci 1962:371–80.
[6] Davis EH. Theories of plasticity and failure of soil masses. In: Lee IK, editor. Soil mechanics selected topics. Elsevier; 1968. p. 341–54.
[7] Davis EH, Booker JR. The bearing capacity of strip footings from the standpoint of plasticity theory. In: Proceedings of the 1st Aust-N.Z. conference on geomechanics. Melbourne; 1971. p. 275–82.
[8] Drescher A, Detournay E. Limit load in translational failure mechanisms for associative and non-associative materials. Géotechnique 1993;43(3):443–56.
[9] Drucker DC, Greenberg W, Prager W. Extended limit design theorems for continuous media. Quart J Appl Math 1952;9:381–9.
[10] Gottardi G, Butterfield R. On the bearing capacity of surface footings on sand under general planar loads. Soils Found 1993;33:68–79.
[11] Hansen JB. A revised and extended formula for bearing capacity. Bull Danish Geotech Inst 1970;28:5–11.
[12] Lyamin AV, Sloan SW. Upper bound limit analysis using linear finite elements and nonlinear programming. Int J Numer Anal Methods Geomech 2002;26(2):181–216.
[13] Lyamin AV, Sloan SW. Lower bound limit analysis using nonlinear programming. Int J Numer Methods Eng 2002;55(5):573–611.
[14] Meyerhof GG. The ultimate bearing capacity of foundations. Géotechnique 1951;2:301–32.
[15] Meyerhof GG. The bearing capacity of foundations under eccentric and inclined loads. In: Proceedings of the third conference of soil mechanics; 1953. p. 440–45.
[16] Michałowski RL. An estimate of the influence of soil weight on bearing capacity using limit analysis. Soils Found 1997;37(4):57–64.
[17] Prandtl L. Über die Härte plastischer Körper Nachrichten von der Geselschaft der Wissenschaften zu Göttingen. Math Phys Klasse 1920;12:74–85.
[18] Reissner H. Zum Erddruckproblem. In: Biezend CB, Burgers JM, editors. Proceedings of the first congress in applied mechanics. p. 295–311.
[19] Salençon J. An introduction to the yield design theory and its application to soil mechanics. Eur J Mech, A 1990;9(5):477–500.
[20] Salençon J, Pecker A. Ultimate bearing capacity of shallow foundations under inclined and eccentric loads. Part I: purely cohesive soil. Eur J Mech A 1995;14(3):349–75.
[21] Salençon J, Pecker A. Ultimate bearing capacity of shallow foundations under inclined and eccentric loads Part II: purely cohesive soil without tensile stress. Eur J Mech A 1995;14(3):377–96.

[22] Sieffert J-G, Bay-Gress Ch. Comparison of European bearing capacity calculation methods for shallow foundations. Geotechnical Engineering. Inst Civil Eng 2000;143(2):65–74.
[23] Sloan SW. Numerical analysis of incompressible and plastic solids using finite elements. PhD Thesis, University of Cambridge; 1981.
[24] Sloan SW, Kleeman PW. Upper bound limit analysis with discontinuous velocity fields. Comput Methods Appl Mech Eng 1995;127:293–314.
[25] Sokolovskii VV. Statics of granular media. Oxford: Pergamon Press; 1965.
[26] Soubra A-H. Upper-bound solutions for bearing capacity of foundations. J Geotech Geoenviron Eng, ASCE 1999;125(1):59–68.
[27] Terzaghi K. Theoretical soil mechanics. New York: Wiley; 1943.
[28] Vesić A. Bearing capacity of shallow foundations. In: Winterkorn HF, Fang HY, editors. Foundation engineering handbook. New York: Van Nostrand Reinhold; 1975. p. 121–47.
[29] Zienkiewicz OC, Humpheson C, Lewis RW. Associated and nonassociated viscoplasticity and plasticity in soil mechanics. Géotechnique 1975;25(4):671–89.